SYNTHESIS AND POWDER X-RAY DIFFRACTION STUDIES OF NOVEL COMPOUNDS RELATED TO BETA-ALUMINA AND MAGNETOPLUMBITE

by

MA'AN HAZEM AMAD

Submitted in Partial Fulfillment of the Requirements

for the Degree of

Master of Science

in Chemistry

Timothy R. Wagner 7/20/94

Advisor Date

Peter J. Kasvinsky 7/22/94

Dean of the Graduate School Date

YOUNGSTOWN STATE UNIVERSITY

JULY 1994

Youngstown State University

Graduate School

Thesis

Submitted in Partial Fulfillment of the Requirements

for the Degree of Master of Science

SYNTHESIS AND POWDER X-RAY DIFFRACTION STUDIES OF NOVEL COMPOUNDS RELATED TO BETA-ALUMINA AND MAGNETOPLUMBITE

Presented by Ma'an Hazem Amad

Accepted by the Department of Chemistry

Timothy R. Wagner — 7/20/94
Major Professor — Date

[signature] — 7/20/94
Professor — Date

Friedrich W. Vahrenkamp — 7/21/94
Professor — Date

[signature] — 7-21-94
Chairman, Chemistry Department — Date

[signature] — 7/22/94
Dean of the Graduate School — Date

ABSTRACT

X-Ray powder diffraction techniques coupled with bond valence analysis were used to provide a description of new magnetoplumbite-type materials synthesized in an effort to determine the extent to which the unusual chemistry observed in $BaGa_{12}O_{19}$ depends on composition, size and identity of the trivalent cation present. The new materials synthesized in this study are $BaAl_3V_9O_{19}$, $BaFe_3V_9O_{19}$, $BaFe_3Nb_9O_{19}$, $BaV_{12}O_{19}$, $BaAl_{2.5}V_{9.5}F_{9.5}N_{9.5}$ and $BaMg_{1.33}Ta_{10.33}N_{19}$. Results of the examination of these compounds using X-ray powder diffraction methods are presented, and show that the only compounds prepared in which the unusual chemistry of $BaGa_{12}O_{19}$ is observed are $BaAl_3V_9O_{19}$, $BaFe_3V_9O_{19}$ and $BaAl_{2.5}V_{9.5}F_{9.5}N_{9.5}$.

The results of a detailed examination of bond lengths and valences of a nitride and mixed nitride-fluoride compound are also presented to predict whether or not nitride and nitride-fluoride analogs to magnetoplumbite-like oxides exist.

ACKNOWLEDGMENTS

My sincere gratitude is extended to my advisor, Dr. Timothy R. Wagner, for his valuable advice, guidance and support during my work. Also I would like to thank Dr. Allen D. Hunter and Dr. Fred Koknat for being on my committee and for their advice. I also thank Dr. James H. Mike and Dr. Jeffrey C. Dick for their support and valuable advice.

A special thanks is also extended to all my friends and to many of my fellow graduate students for their support. Also I would like to thank Ehsan Abu-Dakka for his help during writing this thesis.

Finally, I extend a special thanks to my father, mother and brother and sisters for their love and support which made continuing of study possible.

TABLE OF CONTENTS

LIST OF TABLES

LIST OF FIGURES

LIST OF FIGURES

CHAPTER I

SURVEY OF SOLID-STATE CHEMISTRY

Introduction

Solid-state chemistry is the foundation upon which other solid state sciences are built, since solids must first be synthesized before they can be studied in other disciplines such as solid state physics. However, many fundamental concepts regarding the synthesis of extended solids are lacking. For example, given a certain starting composition, it is not possible at present to predict the final structure of a sample prepared under certain conditions of pressure and temperature. Pursuit of such fundamental knowledge will occupy researchers and theorists for decades to come.

In spite of the lack of a theoretical base for preparing extended solids, the drive to explore the periodic table for new science and technology is strong and cannot wait for answers that may take a long time to come, if ever. Indeed, in the past years, the preparation and examination of new solids led to many technological advances, as well as to an enormous progress in our understanding of material properties. These properties include now commonplace devices and phenomena such as transistors, integrated circuits, lasers, superconductivity, supermagnetism, catalysis and high-strength materials.

Solid-State Materials

Generally solid state materials can be divided into three main groups based on the kinds of bonds that hold the solid together. The first group can be described as molecular solids that consist of small groups of atoms within which the interatomic bonds are strong, but between which the bonds are weak. These weak intermolecular bonds are known as van der Waals bonds and are manifest in the bulk solids by a very small mechanical strength of materials. An example of these molecular solids can be seen in solids that can be easily broken by hand such as candle wax. The second group of solids are called extended solids. These materials are characterized by having strong covalent or ionic bonds which connect one atom to the next in a continuous network from one side of the solid to the other. The third group of solids is known as polymeric solids. These solids are molecular and are characterized by having very long chains of covalently bonded atoms and may have some cross linkage introduced between the long chains.

Of these three groups, the chemistry of extended solids is perhaps the oldest, and conceivably began with the firing of clay pots in prehistoric eras. Yet many basic principles and concepts that serve other branches of chemistry (such as organic) well are lacking or only apply to a small fraction of these solid state compounds. These include the lack of ability to understand and predict the interrelationships between composition, structure, and reaction mechanism from

first principles. In general, our predictive ability is non-existent, slowing the pace of progress in solid state chemistry and making it a science which includes the element of art rather than the use of predictive models.

Unresolved Issues and Long-Term Problems

Since solid state chemistry lacks the theoretical base required to predict interrelationships between composition, structure and reaction mechanism, many challenges at even basic levels remain unsolved. Although theoretical solutions to these problems may be a long time in coming, empirical laws developed by early chemists help in understanding some of these long term problems in solid state chemistry.

One of the greatest accomplishments of early chemists was the development of the law of definite proportions, which states that the ratio of number of atoms in a compound is always expressible as a ratio of integers. Later on, the valence and oxidation state rules were developed to help explain the composition of extended compounds.

In an extended solid both of above rules work reasonably well only for compounds that contain electronegative elements from the right side of the periodic table, combined with electropositive (metallic) elements from the left side of the periodic table. In other words, we can say that the oxidation state rule can explain the occurrence of compounds which contain both electronegative

and electropositive elements. Other compositions of extended solids can be also understood as compounds containing two different oxidation states (variable valence), along with other phenomena, such as the possibility of extensive vacancy formation (a missing atom from a normally occupied position in the structure.) In contrast to the normal valence compounds, there are no general rules that will predict the stoichiometries of intermetallic materials, making our ability to understand the composition of more complicated intermetallic compounds essentially non-existent.

Another central concern of chemistry in extended solids involves the reaction mechanism. In the reaction of solids, there are two main steps for the reaction to take place. First, the atoms must diffuse through the solid precursors to reach an interface between different reactant particles. Second, the atoms must rearrange themselves into the new structure. In extended solids, the relatively slow diffusion mechanism is well studied, however the mechanism by which reactant atoms initially rearrange to form the product structure is almost completely unknown. So the lack of knowledge about the mechanism makes it difficult to explain why a new compound with a new composition does not form in a particular synthesis. An explanation of this problem can be either a thermodynamic or kinetic one. However, in most extended solids the problem might be best explained by thermodynamics. This is due to the necessary

usage of high temperatures in synthesis to enable researchers to obtain reasonable diffusion rates and to promote atom rearrangement.

The crystal structure of extended solid state compounds is an issue which is closely related to composition, but requires more detailed knowledge. In practice, one will be able to experimentally determine the structure of a new compound by X-ray diffraction but will be unable to predict it unless the new compound is a derivative compound. A derivative compound is one which is obtained by replacing one or more elements by chemically similar elements.

FUNDAMENTALS OF X-RAY CRYSTALLOGRAPHY

Introduction

The simplest and most obvious first question to be asked about an inorganic substance is "What is it ?" The methods which are used to ensure this question depend on the nature of the substance. So, if the substance is non-molecular and crystalline, identification is usually carried out by X-ray diffraction, supplemented when necessary by chemical analyses. No single technique is capable of providing a complete characterization of a solid. Therefore, a variety of techniques are used in combination. This work focuses on powder diffraction methods as opposed to single crystal diffraction methods, due to the fact that no single crystal X-ray diffraction facilities are available on campus.

X-ray diffraction has been in use since the early part

of this century for characterization of crystalline materials and for determination of their structure. As a result, X-ray diffraction could be said to be one of the principal techniques of solid state chemistry.

Historical Background

X-Rays are electromagnetic radiation of wavelength approximately 1 Å. They occur in the part of the electromagnetic spectrum which lies between γ and the ultraviolet rays. X-rays are produced when high-energy charged particles collide with matter. The X-ray spectra that are produced usually have two components, a broad spectrum "white radiation" and a number of a monochromatic wavelengths.

In 1895 Röntgen discovered that when high speed electrons were suddenly stopped by matter, a penetrating radiation was emitted. However, the nature of this radiation was a subject of argument for several years. In 1912, Laue, Friedrich and Knipping showed that this radiation had wave properties. The technique of X-ray diffraction was immediately taken up by W.H. and W.L. Bragg. The Braggs employed an experimental technique, in which the diffracted beam was measured as a function of the angle of diffraction by means of an ionization chamber. From the Bragg spectrometer many of the instruments in current use have been developed such as single-crystal cameras and diffractometers, powder cameras and powder diffractometers.

When a single crystal is exposed to X-rays, the three

dimensional array of atoms in the crystal scatters the electromagnetic radiation in such a way that scattered waves reinforce each other only in certain directions. These reflections are governed by Bragg's law:

$$n\lambda = 2d\sin\theta$$

where λ is the wavelength, d is the interatomic spacing, and θ is the angle of reflection at which reinforcement occurs. This can be understood by observing the path of the scattered light in Figure 1 in which the path difference (XYZ) between beam 1 and beam 2 must equal a whole number of wavelengths.

Bragg's law also applies when a monochromatic beam of X-rays strikes a powdered sample. A finely powdered sample will ideally have grains in all possible crystal orientations, and at any given instant, several of these grains will be oriented at a particular set of planes (h,k,ℓ) with an appropriate Bragg angle θ with respect to the X-ray beam.

In the generation of X-rays, a voltage of approximately 35 kV is applied between a cathode and an anode target metal, both of which are placed in a vacuum (Figure 2). When the tungsten filament of the cathode is heated, electrons are released by thermionic emission. These electrons are then accelerated through the vacuum by the large voltage difference between the cathode and the anode. As a result, they gain kinetic energy. However, most of the

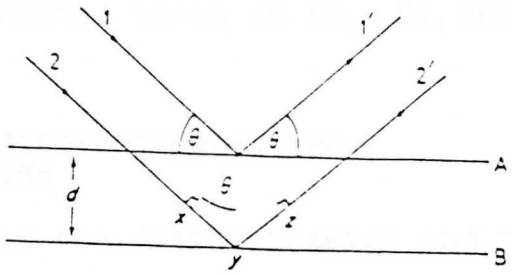

Figure. 1. Conditions of Bragg's Equation, after West[1].

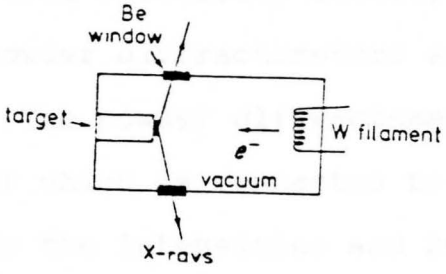

Figure. 2. Schematic design of X-ray tube, after West[1].

kinetic energy (about 98 %) is converted into heat. The nature of X-rays emitted by the X-ray tube will be governed by the elemental composition of the target metal, which will emit several wavelengths known as $K\alpha_2$, $K\alpha_1$ and Kß (Figure 3).

Comparison of the diffractometer and powder camera methods

A comparison of the diffractometer and the powder camera methods shows that the diffractometer possesses a greater resolving power, eliminates film processing and provides a quick scan. By contrast the powder camera is much less expensive, requires less sample and allows weak reflections to be readily detected.

Nowadays, powder camera methods such as the Debye-Scherrer method are used relatively little, and modern computerized X-ray powder diffractometers are supplementing the powder cameras. The powder diffractometer has a Geiger counter as a detector which is connected to a recorder, which in turn records the intensities and 2θ values of the reflections from a specific crystalline powder.

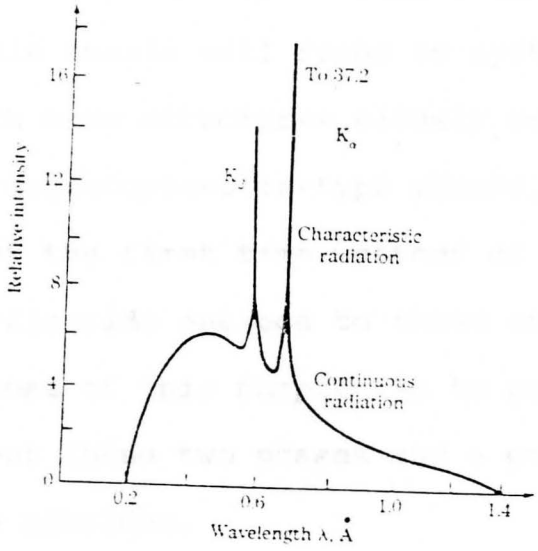

Figure. 3. X-ray emission of a metal, after Smith[2].

CHAPTER II

Survey Of ß-Alumina and Magnetoplumbite Related Phases.

Introduction

ß-alumina and magnetoplumbite (MP) are a group of compounds which consist of "spinel blocks" and "conduction layers," stacked alternately to form a unique layered structure. This thesis will focus on synthesizing related materials which have structures closely related to those of ß-alumina and magnetoplumbite-type phases, and to investigate for the first time whether or not nitride and mixed nitride-fluoride analogs to these compounds exist. Thus, the purpose of this chapter is to provide a general discussion about these two phases and a general description of solid state nitrides.

General Description

Magnetoplumbite (MP) has the ideal composition $2[PbFe_{12}O_{19}]$ per unit cell, while the closely related ß-alumina structure has ideal composition $2[NaAl_{11}O_{17}]$. ß-alumina and magnetoplumbite (MP) both have structures consisting of "spinel blocks" and "conduction layers" which are stacked alternately to form a layered structure. The only difference lies in the contents and the arrangement of ions in the conduction layer. The spinel blocks are

composed of M^{3+} where M is Al^{3+}, Ga^{3+} or Fe^{3+} and O^{2-}, and has the same rigid structure as spinel. For ß-alumina, the conduction plane composition is $(MO)^-$ with M = large cations such as Na^+, K^+, Sr^{2+}, Ba^{2+} or La^{3+} positioned on the spacious conduction layer (Figure 4). For magnetoplumbite, the conduction plane composition is $(MRO_3)^-$ where M is a divalent cation, and R is a trivalent cation.

Historical Background

ß-Alumina was first reported in 1916 by Rankin and Merwin[3] as a new crystallographic form of pure alumina (i.e. Al_2O_3). However, it was soon recognized by Stillwell[4] that a small amount of alkali oxide had to be added to the pure α-alumina in order to produce the observed new crystalline form of alumina, "ß-alumina." Some time later, the X-ray work of Bragg, Gottfried & West[5], and Beevers & Ross[6], established the structure of ß-alumina. Later on, Kummer and Weber[7] discovered that ß-alumina has a high sodium ion conductivity. Generally, ß-alumina will be the name given for the family of compounds of a general formula $MO{\cdot}n(R_2O_3)$ where n can have various values between 5 and 11. The most important member of this family is sodium ß-alumina ($M=Na^+$, $R=Al^{3+}$, $n=6$), which is known to be a byproduct of glass making processes.

Interest in ß-alumina as a solid electrolyte began with work at Ford Motor Company in 1966, where it was found that

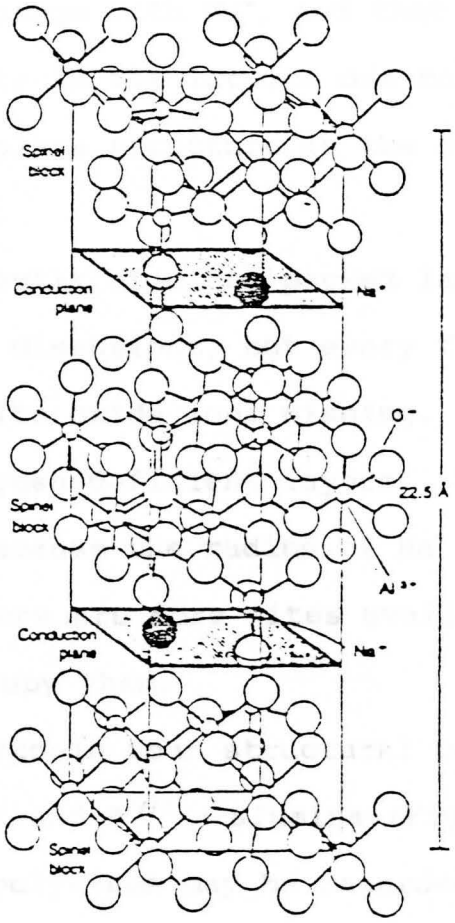

Figure. 4. Structure of one ideal unit cell of ß-alumina, showing Na atoms at the BR sites, after Bates et al.[8].

Na^+ ions are very mobile in the ß-alumina lattice at room temperature and above. Researchers at Ford also showed that divalent cations such as Ba^{2+} could be introduced into the lattice by ion-exchange with Na^+, and that these cations had appreciable mobility in the lattice due to the loosely packed conduction plane structure in the ß-alumina lattice (Figure 5).

ß-Alumina is built of close packed layers of oxide ions stacked into three dimensions, but every fifth layer has three quarters of its oxide ions missing. The Na^+ ions reside in these oxygen-deficient layers. They are able to move very easily because the radius of Na^+ is smaller than that of O^{2-}, and there are more sites available than there are Na^+ ions to occupy them.

ß-Alumina exists in four structural polytypes known as ß, $ß''$, $ß'''$ and $ß''''$ - alumina (Figure 6). The structures of all polytypes may be regarded as built of "spinel blocks" with layers of oxide ions in a cubic stacking sequence of ABCABC. Thus, the structure is closely related to that of spinel, $MgAl_2O_4$, where Al^{3+} ions occupy both tetrahedral and octahedral sites between pairs of adjacent close packed oxygen layers. The adjacent spinel blocks are separated by the oxygen deficient layers, or "conduction bands", where the Na^+ ions reside. The oxide ions in the conduction planes act as bridging ions by bonding to the Al^{3+} ions on either side of the plane.

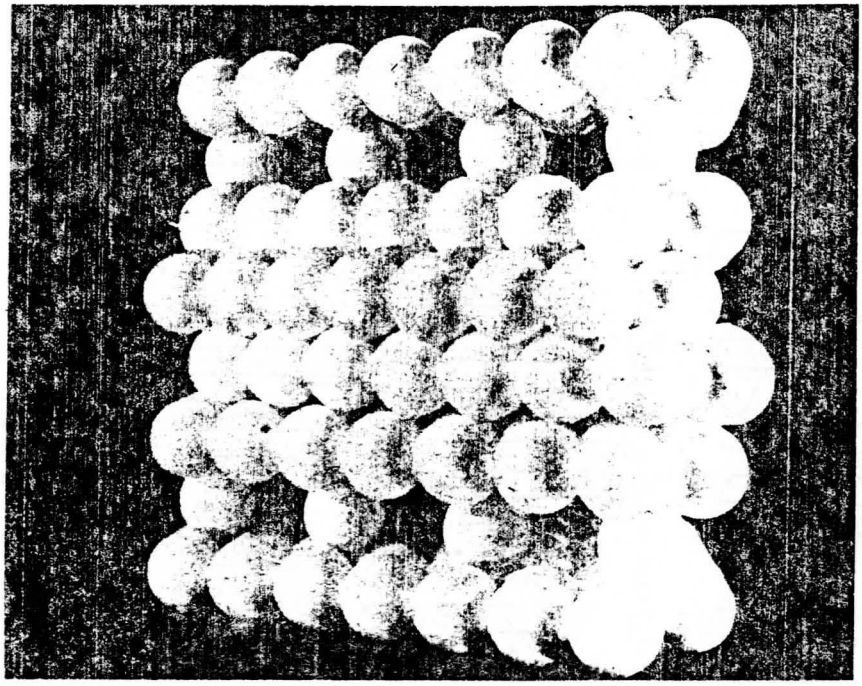

Figure. 5. Oxide layers in ß-alumina, after West[1].

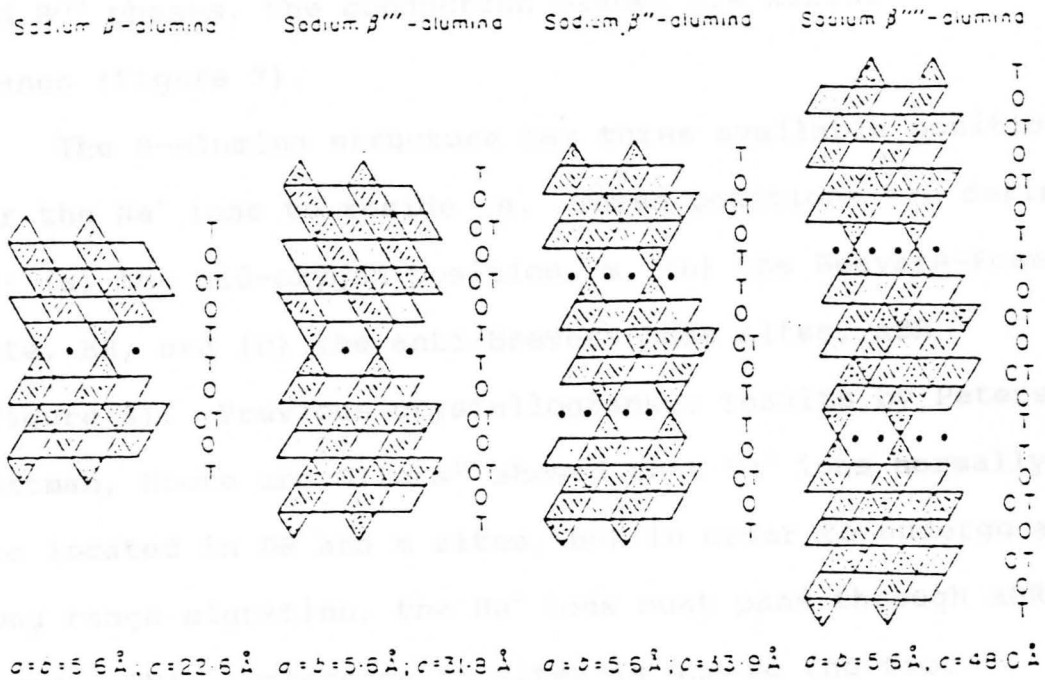

Figure. 6. Structural diagram of the four ß-alumina polytype, after Wagner[9].

The structures of the β''' and β'''' aluminas are very closely related to the structures of β and β'' -alumina, respectively. The major difference between ideal β''' and β-alumina is that the former phase has six oxygen layers per spinel block, while the latter phase has four oxygen layers. This is also the only difference between β'''' and β'', where in this case β'''' has six oxygen layers. Thus, in both β and β''' phases, the conduction planes are mirror planes (Figure 7).

The β-alumina structure has three available positions for the Na^+ ions to reside in. These positions are defined as: (a) the mid-oxygen position, m, (b) the Beevers-Ross site, BR, and (c) the anti-Beevers-Ross sites, aBR (Figure 8). Previous crystallographic results by Peters, Bettman, Moore and Glicks[10] showed that Na^+ ions normally are located in BR and m sites, but in order to undergo any long range migration, the Na^+ ions must pass through aBR sites. This preference in sites is due to the fact that both BR and m sites are larger sites than the aBR site, since the aBR site has an oxygen atom directly above and below it on either side of the conduction plane. So most monocovalent cations prefer to reside in BR and m sites in the β-alumina structure with the exception of the Ag^+ and Tl^+ ions, which show a considerable preference for the aBR sites. This is probably because Ag^+ and Tl^+ ions prefer covalent bonding and sites of low coordination number, such

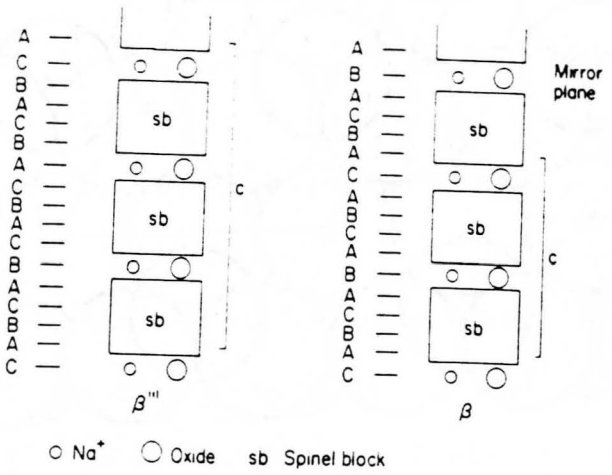

Figure. 7. Oxide packing arrangement showing the mirror plane in ß and ß$^{///}$, after West[1].

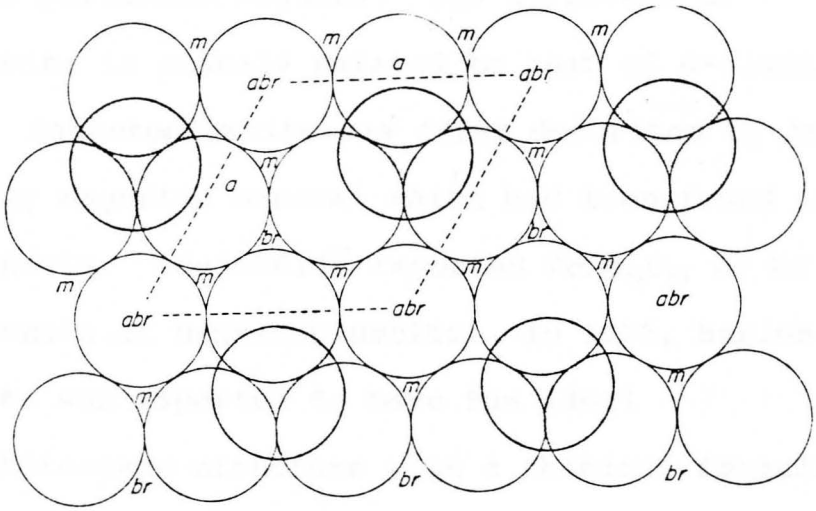

Figure. 8. Conduction plane in ß-alumina; the base of the hexagonal unit cell is shown dashed, after West[1].

as the aBR site.

The unit cell and the space group of ß-alumina was first determined in 1927 by Hendrich and Pauling[11], and it was reported to crystallize in the hexagonal space group $P6_3/mmc$.

Magnetoplumbite is the mineral $PbFe_{12}O_{19}$; its barium analogue, $BaFe_{12}O_{19}$, is known as BaM and is an important component of permanent magnets. The structure of magnetoplumbite is closely related to that of ß-alumina, "$NaAl_{11}O_{17}$". Magnetoplumbite was first described by Aminoff[12] as a strongly magnetic mineral which had been found in the Langban deposits. Adelsköld[13] reported $PbFe_{12}O_{19}$ to be the chemical formula of magnetoplumbite. In 1935, barium hexaaluminate was reported to have the ideal magnetoplumbite-type structure with a chemical formula of $BaAl_{12}O_{19}$. Several years later, it was discovered that this composition does not actually exist. Instead, barium hexaaluminate was found to exist as a two phase material; one phase is barium-poor with respect to $BaAl_{12}O_{19}$, and the other phase is relatively barium-rich.

In 1985, Iyi et al.[14] determined the structure of barium lead hexaaluminate, and found that barium or lead ions are positioned in the centers of the spinel blocks. Later on, Wagner and O'Keeffe[15] showed that barium hexagallate has a disordered barium-rich phase similar to that of barium hexaaluminate, in which some of the barium

ions normally located in the conduction layers of the structure are positioned in the more densely packed layers, as shown in Figure 9.

Barium hexagallate and -hexaaluminate are the only magnetoplumbite-related materials known which have structures involving positioning of large cations in the densely packed layers instead of the conduction planes. X-ray data for $BaGa_{12}O_{19}$ shows the presence of reflections $hk\ell$ and 00ℓ for ℓ = odd in contrast to the requirements that such reflections be absent for compounds with the magnetoplumbite structure. Magnetoplumbite is basically a close packed structure with five oxide layers in a subrepeating unit. Each layer contains four oxide ions per unit cell and the fifth layer contains three-quarters of its quota of oxide ions with large divalent ions such as Pb^{2+}, Ba^{2+} in the other oxide ion sites.

In the magnetoplumbite structure, the aluminum ions of the conduction plane are located in trigonal bipyramidal sites. The bridging Al-O-Al column in ß-alumina changes to two face-shared octahedra in magnetoplumbite, since one oxide ion in the mirror plane of ß-alumina is replaced by three oxide ions (Figure 10).

The magnetic structure of BaM is complex due to the fact that there are Fe^{3+} ions in five different

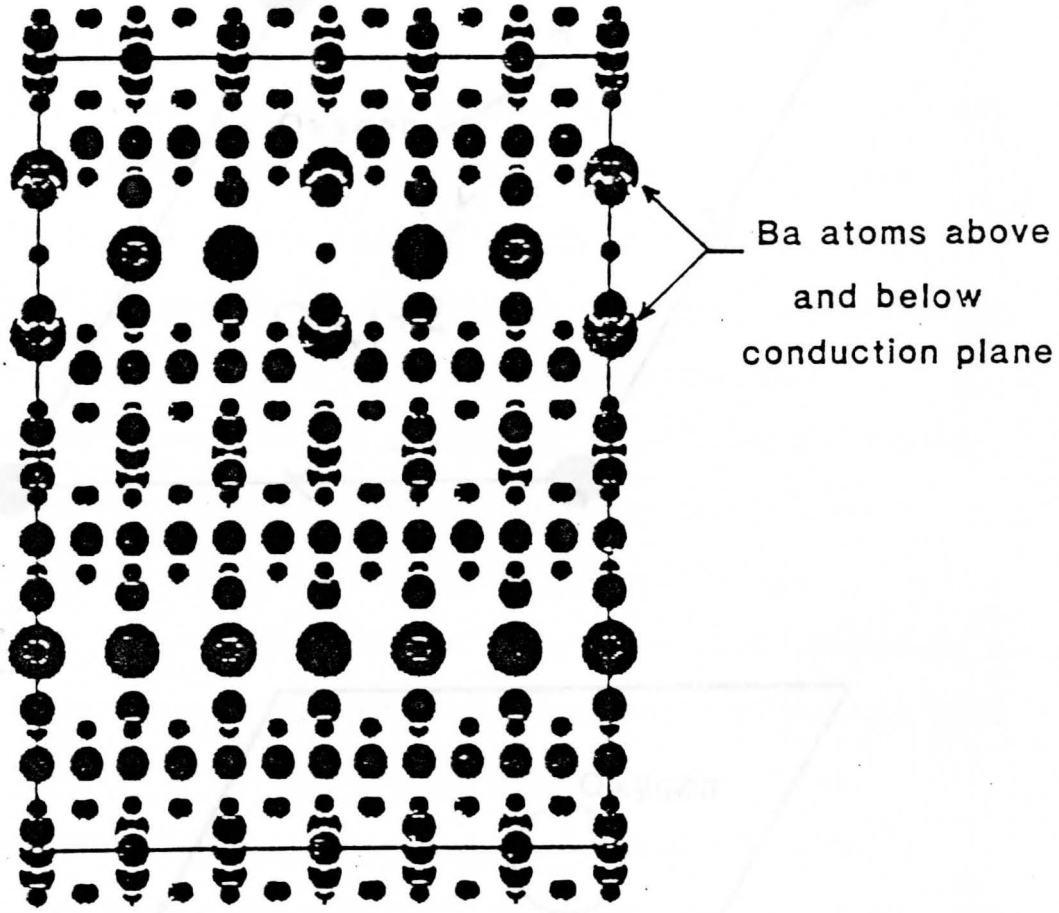

Figure. 9. An atomic plot of the layered-barium model in the [1100] projection, after Wagner[9].

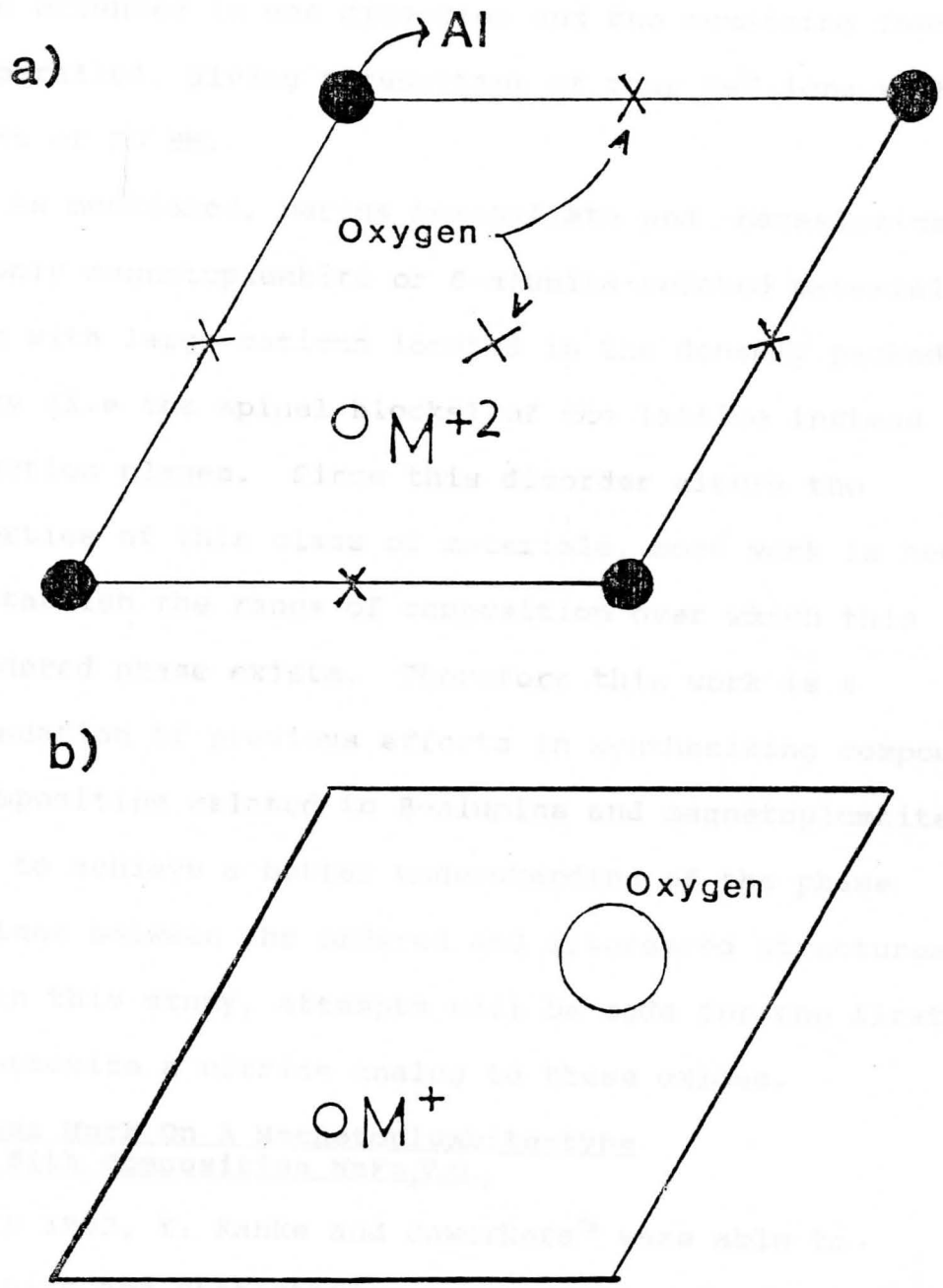

Figure. 10. Planar sketches showing the relative positions of atoms on the conduction plane: a) in magnetoplumbite; b) in ß-alumina.

crystallographic sites. However, the net effect is that in the formula unit $BaFe_{12}O_{19}$, eight of the Fe^{3+} ions have their spins oriented in one direction and the remaining four are antiparallel, giving a resultant of four Fe^{3+} ions with a moment of 20 BM.

As mentioned, barium hexagallate and -hexaaluminate are the only magnetoplumbite or ß-alumina-related materials known with large cations located in the densely packed layers (i.e the spinel blocks) of the lattice instead of the conduction planes. Since this disorder alters the properties of this class of materials, more work is needed to establish the range of composition over which this disordered phase exists. Therefore this work is a continuation of previous efforts in synthesizing compounds of composition related to ß-alumina and magnetoplumbite, in order to achieve a better understanding of the phase relations between the ordered and disordered structures. Also in this study, attempts will be made for the first time to synthesize a nitride analog to these oxides.

Previous Work On A Magnetoplumbite-type Oxide With Composition $NaFe_3V_9O_{19}$

In 1992, Y. Kanke and coworkers[16] were able to synthesize and characterize a magnetoplumbite type oxide of the formula $NaFe_3V_9O_{19}$. The starting materials were ß-$NaFeO_2$, Fe_2O_3, V_2O_4 and V_2O_3, mixed in a 1:1:0.5:4 molar ratio. Thus, one vanadium ion in $NaFe_3V_9O_{19}$ is V^{4+}, so that the composition

is charge-balanced. The structure of $NaFe_3V_9O_{19}$ was determined to be hexagonal with a space group $P6_3/mmc$ with cell parameters of a=5.8388 Å and c=22.8017 Å . This structure was determined by Rietveld refinements of both neutron and X-ray powder data. Kanke and coworkers showed the configuration of coordination polyhedra and Na^+ cations in $NaFe_3V_9O_{19}$ to be as shown in Figure 11.

In previous studies, it has been found that compounds which have c/a ratio > 4.0 most likely adopt a structure closely related to ß-alumina or to that of phase (II) $BaAl_{12}O_{19}$. However, those compounds with c/a ratio < 4 will most likely adopt the magnetoplumbite structure. This is the case for $NaFe_3V_9O_{19}$, for which c/a = 3.9052 using the parameters reported above.

Solid State Nitrides

As mentioned previously, in addition to the oxide materials, attempts will also be made to synthesize a nitride analog to ß-alumina and magnetoplumbite. Such analogs are not known to exist, and successful synthesis of such compounds should lead to a new class of materials with interesting properties.

Nitrides are fascinating materials. Although 78% of the air we breath consists of nitrogen, essentially 100% of the materials making up the earth's crust is made of oxides. Indeed, until recent years, solid state nitride chemistry was neglected due to the fact that nitrides are less stable

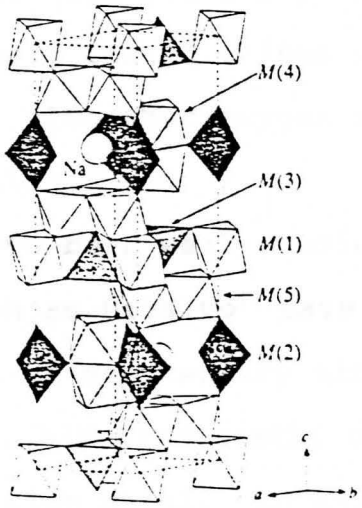

Figure. 11. The structure of $NaFe_3V_9O_{19}$ as proposed by Kanke and coworkers[16]. M(1) octahedral, M(3) tetrahedral, M(4) and M(5) are octahedral.

than oxides. However in the past ten years researchers such as DiSalvo[17] and O'Keeffe[18] investigated analogs of several oxide compounds.

Generally nitrides are less stable than oxides. When heated to high temperatures they lose nitrogen. Also, due to the high bond energy of N_2 molecules compared to O_2 molecules, the decomposition of nitride compounds occurs at lower temperatures. The high stability of oxides relative to nitrides means not only that nitrides must be prepared at lower temperatures, but also that oxygen and water must be excluded from the reaction.

Binary nitrides have been well studied[18]. However, several researchers such as DiSalvo[17] have been active in exploring the formation of new ternary nitrides of the type $M_xL_yN_z$ where M is alkali, alkaline earth, or a rare earth metal and L is a transition metal. In his studies, DiSalvo found that ternary nitrides show an atomic layering (Figure 12) reminiscent of known high-temperature superconductors and a structural versatility that might lead to new superconductors far more tractable than the existing ones[17].

The nitride strategy of this study is to form a nitride analog of magnetoplumbite and test for the presence of the phase by X-ray powder diffraction techniques. Since the nitride compound may not be stable for reasons discussed above, an attempt will also be made to prepare a mixed nitride-fluoride analog. In this material, one N^{3-} and one

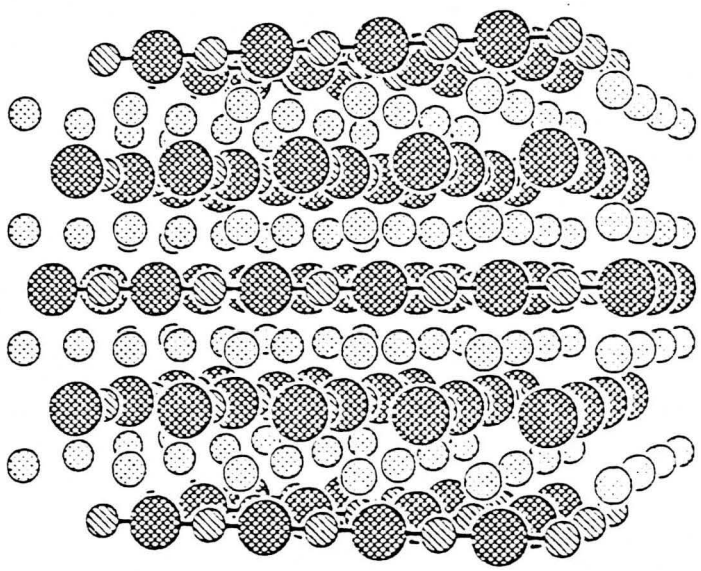

Figure. 12. The structure of CaNiN, showing the atomic layering of the compound. N, represented by the large crosshatched spheres, is bonded to two Ni atoms, as indicated by the connecting lines as proposed by Disalvo[17].

F^- will replace two O^{2-} ions, so that an ideal magnetoplumbite composition would be $MRN_{9.5}F_{9.5}$ (M,R = divalent, trivalent cations, respectively). Finally, this work will investigate whether or not the nitride and mixed fluoride-nitride analogs are likely to exist using the well documented bond-valance sum method. These analyses are discussed in Chapter VI.

CHAPTER III

Statement Of The Problem

This project is a continuation of previous studies[14,15] done on the crystal chemistry of disordered superlattice phases in structures related to magnetoplumbite ($PbFe_{12}O_{19}$) and ß-alumina ($NaAl_{11}O_{19}$). This work will be concerned with the role of the trivalent cation in determining the crystal chemical properties of the ß-alumina/magnetoplumbite system.

Previously (Chapter II), it was mentioned that the compound $NaFe_3V_9O_{19}$ was reported as having the magnetoplumbite structure[16]. The successful synthesis of this compound raises the question as to whether the compound $BaFe_3V_9O_{19}$ exists as an ideal magnetoplumbite, or as a disordered superstructure similarly to $BaGa_{12}O_{19}$. To investigate, it is proposed to synthesize $BaFe_3V_9O_{19}$ and analyze the newly prepared compound utilizing the X-ray powder diffraction method. X-ray data should not only verify whether or not a ß-alumina/magnetoplumbite phase was formed, but should also indicate whether or not the phase is likely to be disordered, as discussed later. An attempt to synthesize $BaFe_3Nb_9O_{19}$ is also proposed, to investigate the structural effects of the large Nb^{3+} ion. In addition, $BaAl_3V_9O_{19}$ will be prepared, to determine whether or not the smaller Al^{3+} ion (compared to Fe^{3+}) has an effect relative to the observed crystal properties of $BaFe_3V_9O_{19}$. Finally, $BaV_{12}O_{19}$ will be prepared as an analog to $BaGa_{12}O_{19}$. It should

be noted that none of the compounds proposed to be studied have been previously reported.

Also, this work will investigate for the first time whether or not nitride and mixed nitride-fluoride analogs to the magnetoplumbite phase exists. The possible existence of the nitride and nitride-fluoride analogs will be further investigated in this study using the well documented bond-valence sum method[19].

Chapter IV

Experimental Methods.

Introduction

The techniques used in obtaining the results in this project can be divided into two major categories: 1) Sample preparation; and 2) Sample analysis by X-ray powder diffraction methods, coupled with computer analysis. A program used for computer analysis of the X-ray data will be explained later in this section.

Sample Preparation

Standard ceramic techniques were used to synthesize the newly prepared materials. This method involves mixing stoichiometric amounts of the starting materials, followed by annealing at an appropriate temperature for seven to eight days. The starting materials were carefully ground into a fine powder in an agate mortar, and then weighed using a digital balance to the third decimal place. The fine powder was thoroughly mixed in an acetone suspension, creating a slurry, and the mixture was typically left in air for one hour to evaporate the acetone. The fine powder was then heated to 400 ^{0}C in an evacuated quartz tube for one day to evolve CO_2 gas from the metal carbonate starting materials. After the first heating, the powder was mixed well in an acetone slurry, pressed into pellets, placed in an α-alumina crucible, and then placed in an evacuated

quartz tube and heated at the necessary temperature for seven days.

Nitride compounds were prepared similarly, except that samples were heated in a nitrogen atmosphere, rather than in vacuo.

X-Ray Powder Diffraction

X-ray powder diffraction was used to determine whether the desired solid state reaction went to completion, and also to determine whether or not the compounds prepared had the magnetoplumbite phase.

X-ray powder diffraction data were collected at room temperature on a Rigaku Geiger counter diffractometer D/Max-A Series, using Cu Kα radiation. Samples for X-ray analysis were prepared by first crushing the annealed pellet into a fine powder in an agate mortar, followed by creating a slurry in an acetone suspension. The solid obtained from the evaporation of the acetone suspension was ground into a fine powder and then mounted on a glass holder. The d-spacings were calculated for each pattern and then indexed by means of computer analysis.

Computer Analysis

The program used for indexing the X-ray powder diffraction pattern for a given crystal system was written by Mr. Ehsan Abu-Dakka. A copy of the program is listed on the next page.

The program indexes each reflection for a given unit cell parameter and calculates all the d-spacings and 2θ

```
          program find (input, outpuy, out_file);
var
   out_file:
       text;
       h, k, l, n:
            integer;
       a, c, j, m, dinv, d, con, sin_theta, angle, lambda:
            real;
     function theta (arg:real): real;
     const
          pi = 3.1415;
     var
           cos, sin, tan_angle, theta_rad: real;
     begin
         cos := sqrt (abs (1 - sqr (arg)));
         tan_angle := arg / cos;
         theta_rad := arctan (tan_angle);
         theta :=180 * theta_rad / pi;
        end;
     begin (* main *)
          assign (out_file, 'b:out_file.dat');
          rewrite (out_file);
          write (' Enter the value of the constant a:  ');
          readln (a);
          write (' Enter the value of the constant c:  ');
          readln (c);
          write (' Enter the value for Lambda:         ');
          readln (lambda);
          con := lambda / 2;
          writeln (out_file , 'h':10, 'k':10, 'L':10, 'd':10, '2
* theta':10);
          j := 4 / (3 * sqr (a));
          for h := 0 to 5 do
            for k := 0 to 5 do
            for l := 1 to 9 do
                begin
                  n := sqr (h) + h * k + sqr (k);
                  m := sqr (l) / sqr(c);
                    dinv := sqrt (j * n + m);
                  d := 1 / dinv;
                  write (out_file, h:5, k:5, l:5);
                  write (out_file, 'd = ', d:5:4);
                  sin_theta := con * dinv;
                  angle := 2 * theta (sin_theta);
                  writeln (out_file, '2 theta = ':5, angle:5:5);
                end;
      end.
```

angles for reflections of all hkℓ values within a chosen range .

The 2θ angles calculated by computer were compared with the 2θ angles obtained from the diffraction patterns. A match was accepted when the observed 2θ was found to be within a default limit of 0.1 degrees of the calculated value.

CHAPTER V

Experimental Results

Introduction

The major goal of this chapter is to provide a description of the newly synthesized materials with starting compositions related to magnetoplumbite. Beside the synthesis of the compounds, the majority of the work done in this study involved the X-ray analysis of the compounds prepared. From the X-ray data, it can be determined whether the newly synthesized compounds have the magnetoplumbite phase, or if they exist in two or more different phases.

Table 1 lists the cell parameters a and c obtained from the X-ray powder diffraction data taken from compounds prepared in this study. Also shown for comparison is the previously prepared compound $NaFe_3V_9O_{19}$. Note that the compositions listed in the Table represent the ideal starting compositions of each compound. Actual compositions may vary slightly, and can be determined only through microanalysis techniques, as discussed later. The method of obtaining the cell parameters was described in Chapter IV. The ratio of c/a is also given in the table. Previously it was mentioned that those compounds which have $c/a > 4.0$ are closely related to ß-alumina, while those compounds with c/a less than 4.0 most likely adopt the magnetoplumbite structure. Kummer[20] noted that the c value of the

TABLE 1

Cell parameters a and c and c/a of compounds synthesized in this study.

Compound	a(Å)	c(Å)	c/a
$BaV_{12}O_{19}$	5.7564	24.142	4.1940
$BaAl_3V_9O_{19}$	5.6534	22.287	3.9422
$BaFe_3V_9O_{19}$	5.833	22.872	3.9211
$BaFe_3Nb_9O_{19}$	5.8259	23.495	4.0328
$BaAl_{2.5}(VFN)_{9.5}$	5.9492	23.573	3.9625
*$NaFe_3V_9O_{19}$	5.8388	22.8017	3.9052

* Results obtained from Kanke et al.[16].

lattice parameters becomes larger as the radius of the monovalent cation in the conduction plane increases, and this would explain why c/a tends to be larger for ß-alumina-type compounds (which ideally have M^+ on conduction planes) than it is for magnetoplumbite-type compounds (which ideally have M^{2+} in their conduction planes). Furthermore, Newsam and Tofield[21] and Boilot et al.[22], described the tendency of the c parameter to decrease according to the increase in the cation population in the conduction layer. Since the composition of the conduction plane in magnetoplumbite-type compounds is $[MNO_3]^-$ (N=trivalent cation), while that for ß-alumina is $[MO]^-$, one would expect the c/a ratio to be smaller for magnetoplumbite compounds.

In short, the magnetoplumbite structure becomes favorable as the charge of the cation on the mirror plane increases (size decreases), and the ß-alumina structure becomes more stable as the cation size increases. Although exceptions to the empirical c/a ratio rule could be possible, many compounds do follow this trend[20]. For example, Table 1 shows that c/a for $NaFe_3V_9O_{19}$ is 3.9052[12]. This compound is closely related in composition to compounds prepared in this study, and was reported by neutron and X-ray diffraction studies as having the magnetoplumbite structure. Therefore the c/a ratio will be used as a guideline in this work to predict which phase (i.e. magnetoplumbite or ß-alumina, if either) the synthesized compounds adopt.

$BaAl_3V_9O_{19}$

$BaAl_3V_9O_{19}$ was prepared by mixing stoichiometric amounts of the starting materials, $BaCO_3$, Al_2O_3 and V_2O_3 . About 3 grams of the mixture was placed in an α-alumina crucible, which in turn was placed in an evacuated quartz tube and heated for one day at 769 ^{0}C. After cooling to room temperature, the product was ground and identified by X-ray powder diffraction with monochromatized Cu K_α radiation. The resulting sequence of X-ray patterns obtained is shown in Figures 13-16. This procedure was repeated until the X-ray pattern no longer changed. Two heating runs (1+3 days) were required to obtain pure $BaAl_3V_9O_{19}$.

The X-ray powder diffraction data for $BaAl_3V_9O_{19}$ is shown in Table 2, and the corresponding diffraction pattern is shown in Figure 16. From this data, it is seen that this compound exists as a single phase, adopting the magnetoplumbite/ß-alumina structure. The reflections are indexed according to the hexagonal parameters given in Table 1. The c/a ratio of 3.9422 suggests the presence of a magnetoplumbite-like structure. However, the presence of the forbidden reflections (for space group $P6_3/mmc$) $hk\ell$ and 00ℓ for ℓ = odd indicates that this compound cannot have the ideal magnetoplumbite structure, as similarly observed for $BaGa_{12}O_{19}$ and $BaAl_{12}O_{19}$.

It is evident from Table 2 and from Figure 16 that a single phase is present in the sample. This is supported by the similarity between the calculated and observed 2θ shown

TABLE 2

Powder X-Ray Diffraction Data For
$BaAl_3V_9O_{19}$.

h	k	ℓ	2θ(cal)	2θ(obs)
0	0	2	7.92	7.90
* 0	0	3	11.90	11.90
0	0	4	15.80	15.80
1	0	1	18.53	18.50
1	0	2	19.79	19.80
0	1	2	19.79	19.80
* 0	0	5	19.90	19.90
0	1	3	21.72	21.70
0	0	6	23.93	23.90
0	1	4	24.17	24.10
0	1	5	27.00	27.00
0	0	7	28.00	28.00
1	0	6	30.17	30.10
0	0	8	32.10	32.10
0	1	7	33.54	33.50
* 0	0	9	36.24	36.20
0	2	1	36.90	36.90
2	0	1	36.90	36.90
1	0	8	37.09	37.01
0	2	2	37.58	37.50
1	1	6	40.10	40.05
2	0	4	40.20	40.20
1	0	9	40.80	40.89
1	1	7	42.75	42.80
1	1	8	45.68	45.70

TABLE 2
(continuation)

Powder X-Ray Diffraction Data For
$BaAl_3V_9O_{19}$.

h	k	ℓ	2θ(cal)	2θ(obs)
1	2	2	49.91	49.90
1	2	4	52.03	52.10
1	2	6	55.42	55.50
3	0	2	56.98	58.90
0	3	4	58.90	58.90
0	3	7	64.06	64.10
1	3	3	70.43	70.40

* Forbidden reflection for ideal magnetoplumbite structure (space group $P6_3/mmc$).

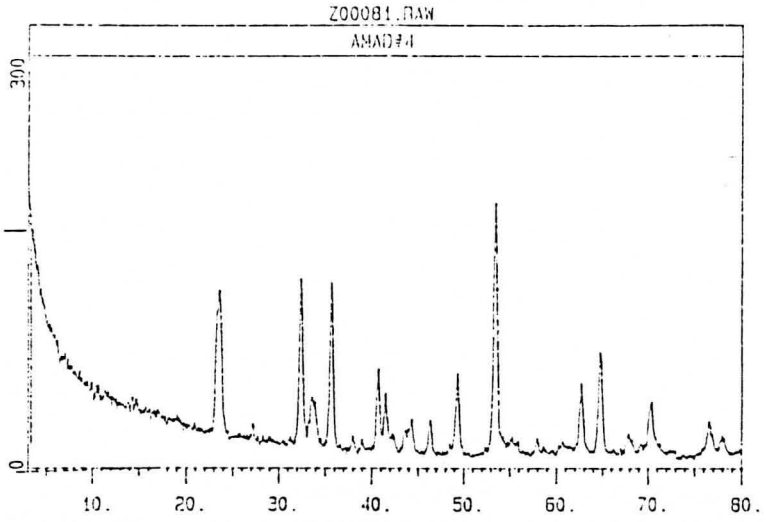

Figure. 13. X-ray diffraction pattern of unfired $BaAl_3V_9O_{19}$.

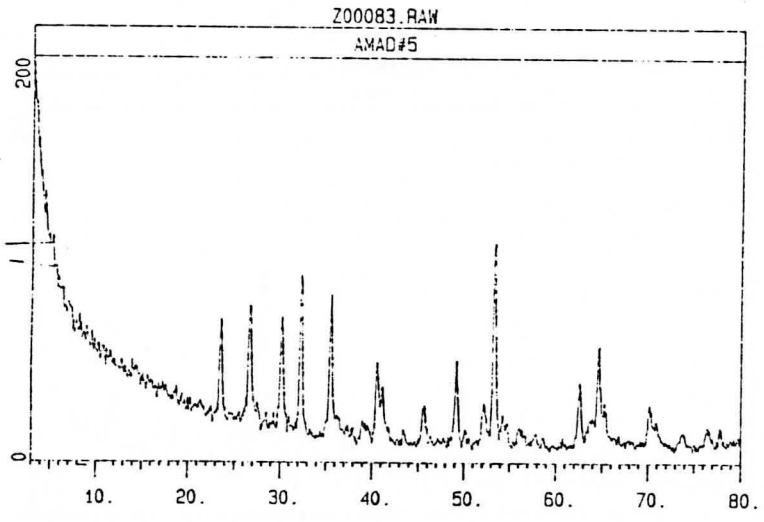

Figure. 14. X-ray pattern of $BaAl_3V_9O_{19}$ fired for one day.

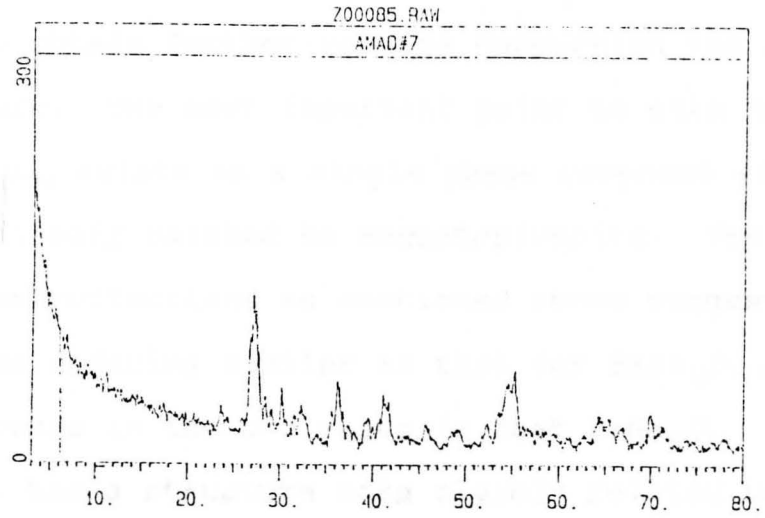

Figure. 15. X-ray pattern of $BaAl_3V_9O_{19}$ fired for 2 days.

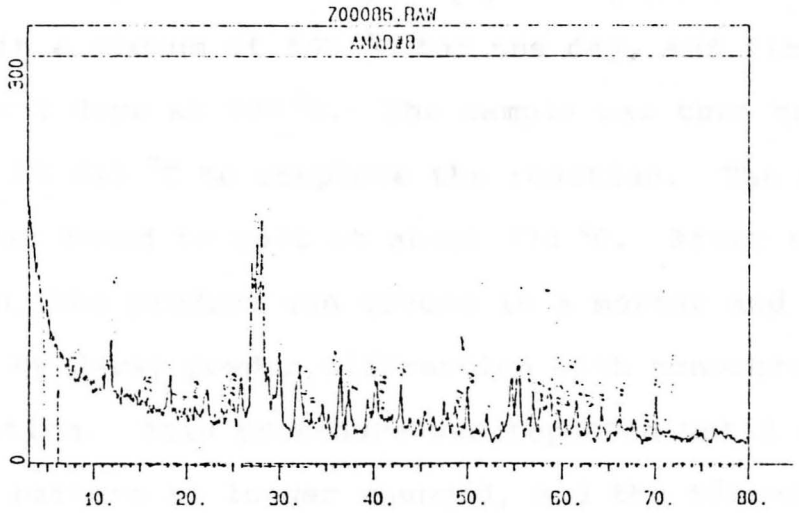

Figure. 16. X-ray pattern of $BaAl_3V_9O_{19}$ fired for 6 days.

in Table 2. However, transmission electron microscopy (TEM) and single crystal X-ray diffraction studies will be required to obtain further results concerning the details of the structure. The most important point to make here is that $BaAl_3V_9O_{19}$ exists as a single phase compound with a structure closely related to magnetoplumbite. The presence of forbidden reflections as mentioned above suggests a superlattice ordering similar to that for $BaGa_{12}O_{19}$. The only difference in the two cases is that $BaGa_{12}O_{19}$ (c/a 4.063) has a structure more closely related to ß-alumina.

$BaFe_3V_9O_{19}$

$BaFe_3V_9O_{19}$ was prepared by mixing stoichiometric amounts of the starting powders ($BaCO_3$, Fe_2O_3 and V_2O_3), followed by annealing in a vacuum at 565 ^{0}C for one day, and finally heating for 3 days at 585 ^{0}C. The sample was then heated for 2 days at 615 ^{0}C to complete the reaction. The product $BaFe_3V_9O_{19}$ was found to melt at about 720 ^{0}C. After each heating run, the product was ground in a mortar and identified by X-ray powder diffraction with monochromatized Cu K_α radiation. This procedure was repeated until the X-ray powder pattern no longer changed, and the time-sequence of X-ray patterns is shown in Figures 17-20.

X-ray data for this compound is shown in Tables 3 and 4, and the corresponding X-ray pattern is shown in Figure 20. From this data, it could be suggested that this compound exists as two phases, a magnetoplumbite-like phase

TABLE 3

X-Ray Powder Diffraction Data For $BaFe_3V_9O_{19}$.

h	k	ℓ	2θ(cal)	2θ(obs)
0	0	2	7.73	7.74
* 0	0	3	11.61	11.62
0	1	1	17.98	17.94
* 0	0	5	19.33	19.29
1	0	5	26.28	26.20
0	0	7	27.29	27.30
0	1	6	29.35	29.36
0	0	8	31.28	31.30
1	1	2	31.66	31.66
0	1	7	32.64	32.64
* 0	0	9	35.31	35.30
0	2	2	36.43	36.40
0	2	3	37.51	37.50
0	2	5	40.81	40.52
1	1	7	41.50	41.50
0	2	6	42.95	42.96
0	2	7	45.38	45.38
2	1	4	50.38	50.36
1	2	6	53.69	53.64
0	3	1	54.65	54.62
1	2	7	55.76	55.70
3	0	5	58.39	58.38
0	3	7	62.00	62.02
0	3	9	66.62	66.64
1	3	5	70.26	70.28

* Forbidden reflection for ideal magnetoplumbite structure (space group $P6_3/mmc$).

TABLE 4

Unindexed Peaks in the X-ray Powder Diffraction Data For $BaFe_3V_9O_{19}$ that Indicate the Presence of a Fe_2O_3 Phase.

N	* 2θ(cal)	2θ(obs)
1	24.71	24.62
2	29.75	29.76
3	32.65	32.64
4	37.50	37.50
5	45.31	45.38
6	50.36	50.36

* Calculated using cell parameters from JCPDS card # 21-920.

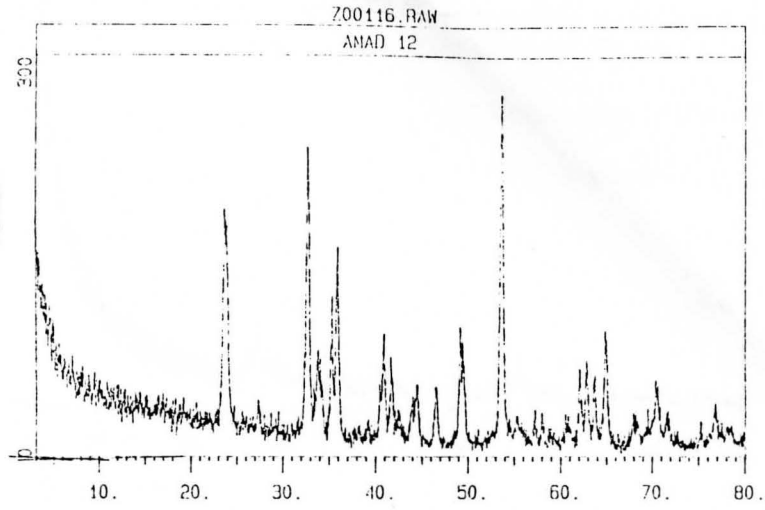

Figure. 17. X-ray pattern for unfired $BaFe_3V_9O_{19}$.

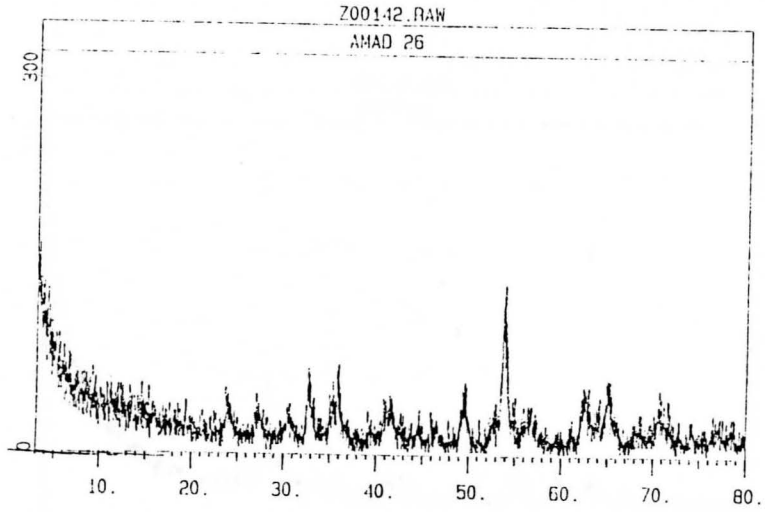

Figure. 18. X-ray pattern of $BaFe_3V_9O_{19}$ fired for 1 day.

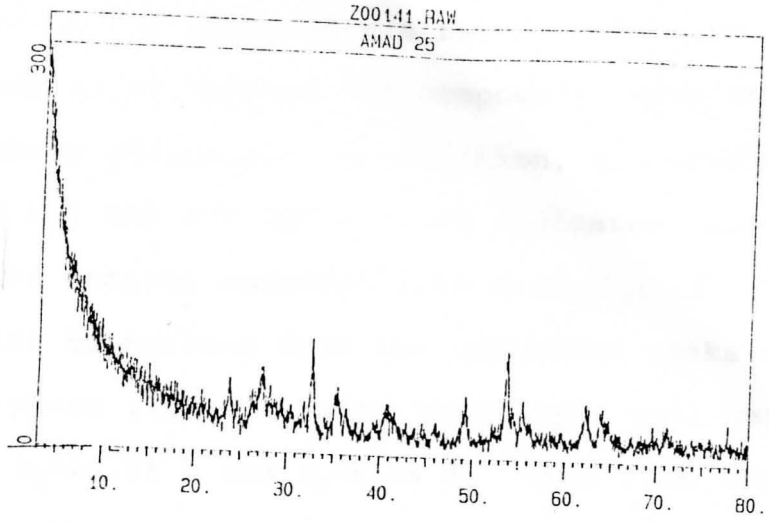

Figure. 19. X-ray pattern for $BaFe_3V_9O_{19}$ fired for 4 days.

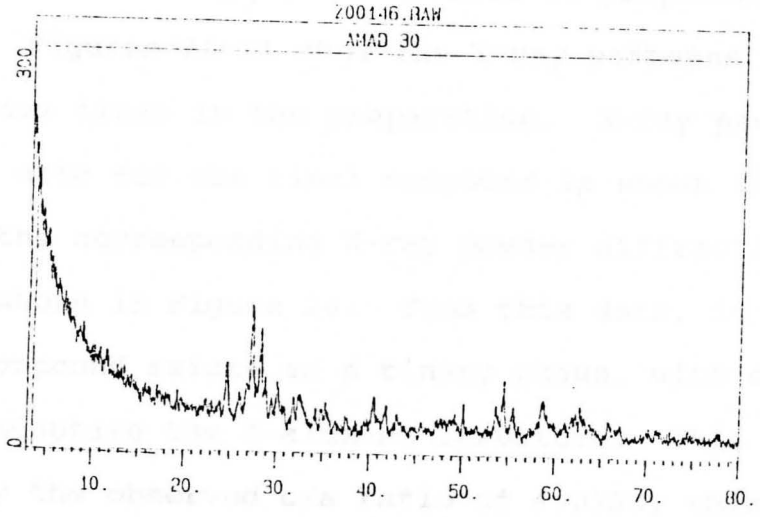

Figure. 20. X-ray pattern of $BaFe_3V_9O_{19}$ fired for 6 days.

and Fe_2O_3. The presence of a magnetoplumbite-like phase can be supported by the observed c/a ratio of 3.92109. This ratio is seen to be typical for compounds known to have the magnetoplumbite structure. In addition, the presence of the reflections hkℓ and 00ℓ for ℓ = odd indicates that this compound also behaves somewhat like $BaGa_{12}O_{19}$. From Table 3, it could also be noticed that the unindexed peaks correspond to an Fe_2O_3 phase (Table 4) with monoclinic cell parameters a_0=12.97 Å, b_0=10.21 Å and c_0=8.44 Å. Thus from the X-ray data (Figure 20), it appears to be evident that $BaFe_3V_9O_{19}$ exists as two phases: a magnetoplumbite/ß-alumina structure with a superlattice, and Fe_2O_3 .

$BaFe_3Nb_9O_{19}$

Due to the difficulty in obtaining Nb_2O_3, NbO and NbO_2 were used instead in equimolar amounts in preparing $BaFe_3Nb_9O_{19}$. Figures 21-24 show the X-ray patterns taken during various times in the preparation. X-ray powder diffraction data for the final compound is shown in Tables 5 and 6, and the corresponding X-ray powder diffraction pattern is shown in Figure 24. From this data, it is seen that this compound exists as a binary phase, with one phase apparently adopting the ß-alumina structure. This is supported by the observed c/a ratio of 4.0328, which is seen to be typical for compounds known to have ß-alumina structure. X-ray data shown in Table 5 indicate that forbidden reflections for $P6_3/mmc$ are not observed. Here the reflections are indexed according to the hexagonal

TABLE 5

Powder X-Ray Diffraction Data For
$BaFe_3Nb_9O_{19}$.

h	k	ℓ	2θ(cal)	2θ(obs)
0	0	2	7.53	7.50
0	0	4	15.08	15.01
0	1	1	17.98	17.98
0	1	3	20.94	20.94
0	1	4	23.24	23.24
0	0	7	26.55	26.56
0	1	6	28.86	28.86
0	0	8	30.43	30.32
1	1	3	32.80	32.76
0	1	8	35.36	35.30
0	2	2	36.43	36.40
0	2	7	44.95	44.90
0	2	9	50.29	50.30
1	2	4	50.29	50.30
1	2	6	53.44	53.28
0	3	1	54.71	54.74
3	0	1	54.71	54.74
3	0	7	61.69	61.60
1	3	5	70.17	70.17
1	3	9	77.37	77.32

TABLE 6

The Unindexed Peaks in the X-ray Diffraction Data for $BaFe_3Nb_9O_{19}$ that Might Indicate the Presence of $BaFe_2O_4$ Phase.

N	* 2θ(cal)	2θ(obs)
1	21.44	22.32
2	---	24.14
3	30.35	29.60
4	---	42.10
5	42.46	42.36
6	45.45	45.62
7	49.61	49.28
8	55.91	55.84
9	---	64.46
10	69.92	69.91

* Calculated using cell parameters from JCPDS card # 20-132.

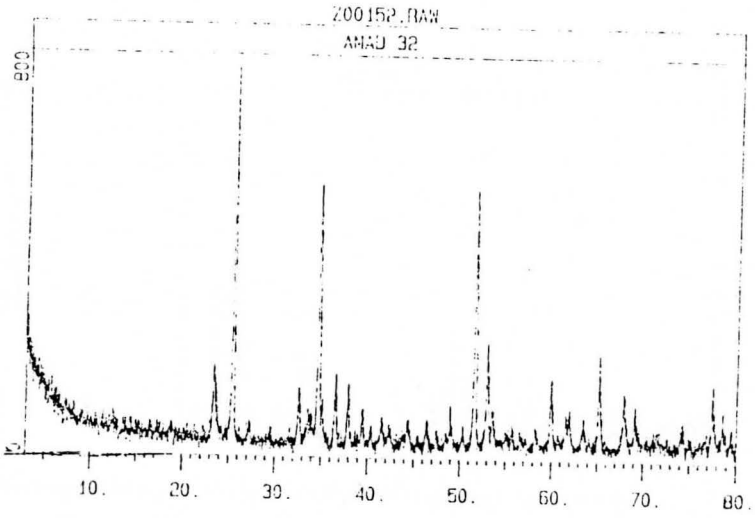

Figure. 21. X-ray pattern for unfired $BaFe_3Nb_9O_{19}$.

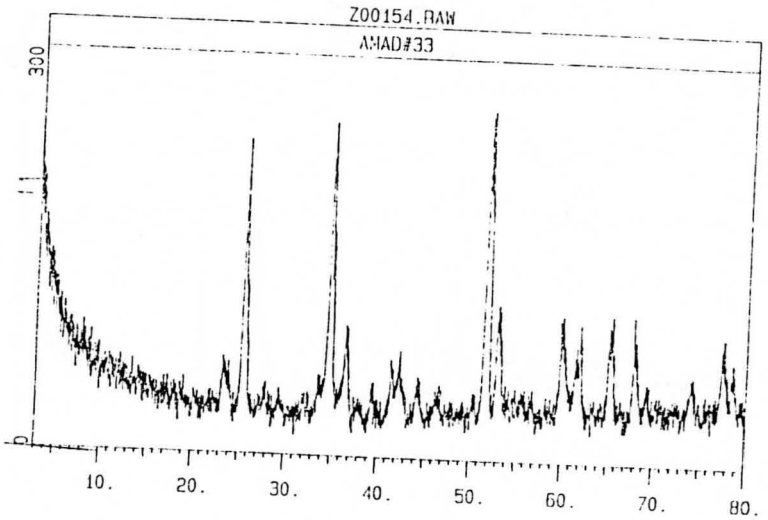

Figure. 22. X-ray pattern of $BaFe_3Nb_9O_{19}$ fired for 1 day.

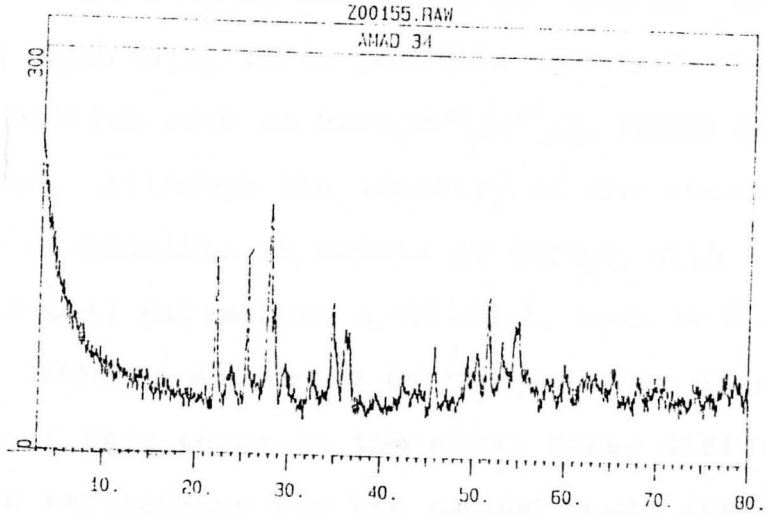

Figure. 23. X-ray pattern for $Ba_3Nb_9O_{19}$ fired for 3 days.

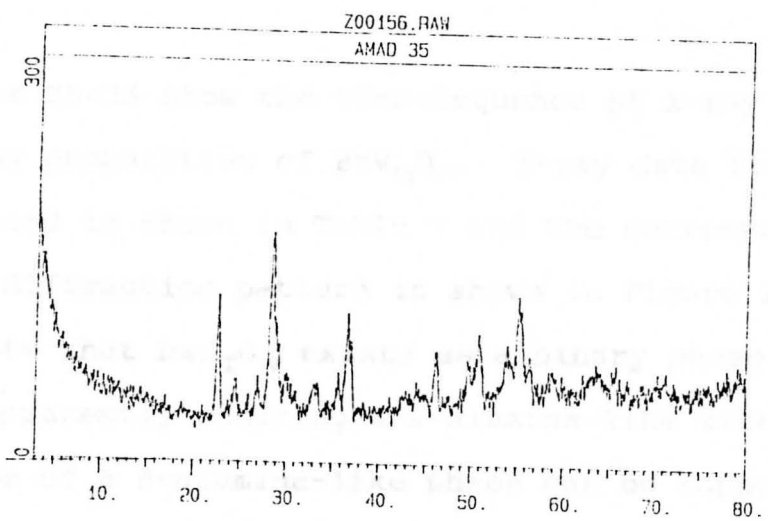

Figure. 24. X-ray pattern for $BaFe_3Nb_9O_{19}$ fired for 5 days.

parameters given in Table 1.

It is evident from Figure 24 that more than one phase is present in the sample, and since Nb^{+2} and Nb^{+4} were used as starting materials, it is possible that a ß-alumina phase with a composition such as $BaFe_2Nb^{+2}{}_5Nb^{+4}{}_4O_{17}$ forms as a primary phase. Although the identity of the second phase is unclear, it is possible it exists as $BaFe_2O_4$ with orthorhombic cell parameters a_0=19.05 Å, b_0=5.39 Å and c_0=8.448 Å. This is supported by the presence of some reflections of this phase in the final X-ray diffraction pattern. The reflections for the second phase are given in Table 6.

In this case, the phase relationships could be further elucidated using other techniques such as TEM.

$BaV_{12}O_{19}$

Figures 25-28 show the time-sequence of X-ray patterns taken during preparation of $BaV_{12}O_{19}$. X-ray data for the final compound is shown in Table 7 and the corresponding X-ray powder diffraction pattern is shown in Figure 28. The data suggests that $BaV_{12}O_{19}$ exists as a binary phase, with one phase apparently adopting a ß-alumina-like structure. The presence of a ß-alumina-like phase can be supported by the observed c/a ratio of 4.1940 (i.e > 4.0), which is seen to be typical for compounds known to have the ß-alumina structure. The second phase was identified to possibly be VO_2. This was supported by the presence of two reflections of a VO_2 phase with triclinic cell parameters of a_0=5.80 Å,

TABLE 7

Powder X-Ray Diffraction Data For
$BaV_{12}O_{19}$.

h	k	ℓ	2θ(cal)	2θ(obs)
* 0	0	1	3.56	3.60
0	0	4	14.29	14.29
0	1	6	27.90	27.90
1	1	3	32.56	32.60
0	2	1	35.74	35.67
1	1	5	35.72	35.67
1	1	7	40.05	40.04
0	2	5	40.07	40.04
0	2	6	41.92	41.86
1	2	2	48.23	48.18
0	2	9	48.93	48.91
1	2	3	48.93	48.91
1	2	7	54.61	54.62
0	3	1	54.64	54.62
0	3	2	55.05	54.99
3	0	4	56.66	56.68
1	2	9	58.86	58.87
0	3	6	59.27	59.23
2	2	2	64.33	64.33
0	3	9	64.91	64.94
2	2	5	66.89	66.88
3	1	2	67.26	67.25
2	2	6	68.21	68.22
1	3	6	71.06	71.13
1	3	8	74.31	74.29
1	3	9	76.25	76.24
0	4	3	76.29	76.24
0	4	4	77.08	77.09

* Forbidden reflection for ideal magnetoplumbite (space group $P6_3/mmc$).

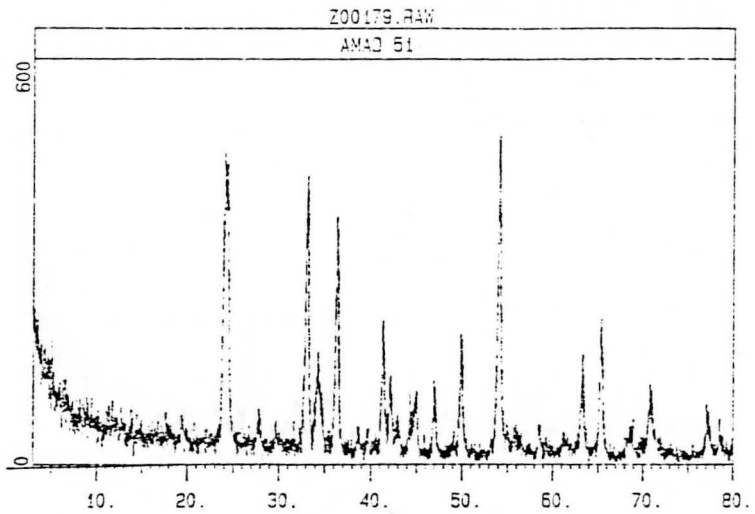

Figure. 25. X-ray pattern for unfired $BaV_{12}O_{19}$.

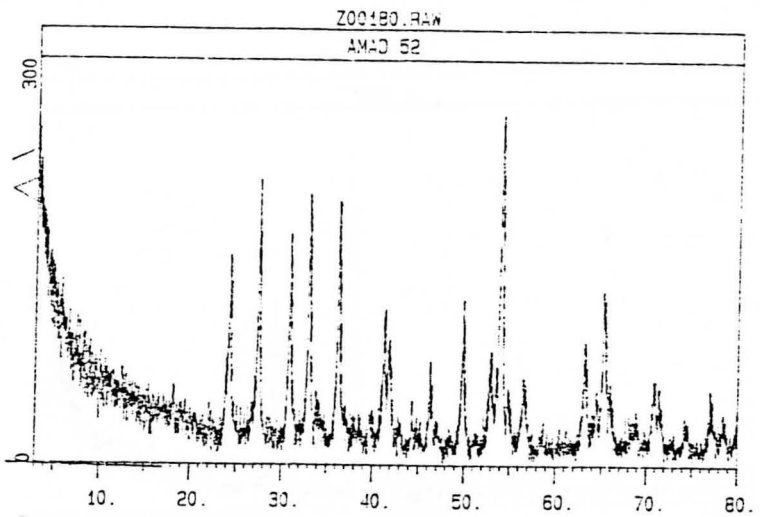

Figure. 26. X-ray pattern of $BaV_{12}O_{19}$ fired for 1 day.

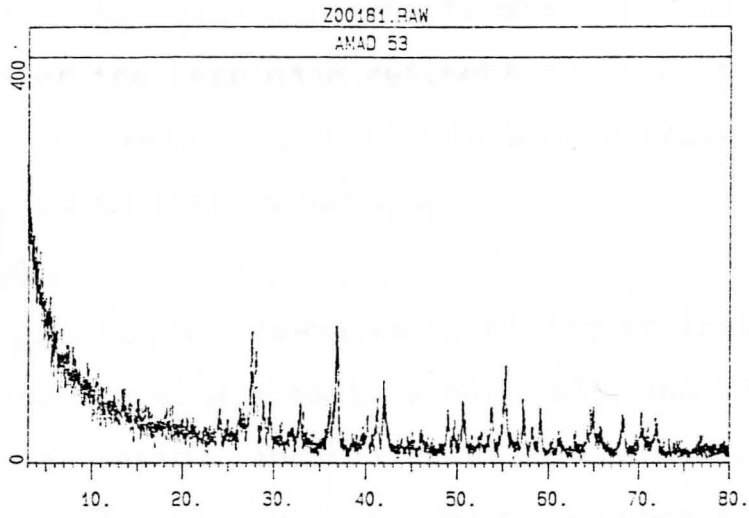

Figure. 27. X-ray pattern of $BaV_{12}O_{19}$ fired for 4 days.

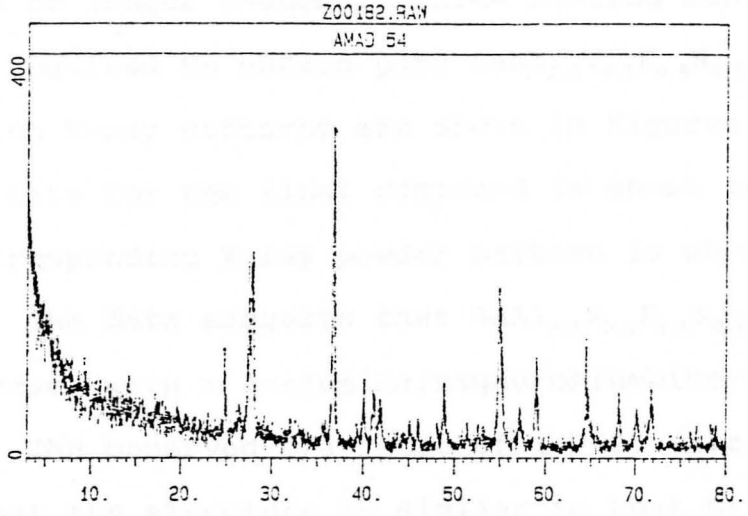

Figure. 28. X-ray pattern of $BaV_{12}O_{19}$ fired for 7 days.

b_0=4.52 Å and c_0 5.58 Å (JCPDS CARD # 33-1441) in the final X-ray powder diffraction pattern (Figure 28). In view of the presence of the forbidden reflection 001 in the X-ray data for $BaV_{12}O_{19}$, this compound could have a structure very closely related to that of $BaGa_{12}O_{19}$.

$BaAl_{2.5}V_{9.5}F_{9.5}N_{9.5}$

$BaAl_{2.5}V_{9.5}F_{9.5}N_{9.5}$ was prepared by mixing stoichiometric amounts of the starting materials BaF_2, AlF_3 and VN in a 1:2.5:9.5 molar ratio. About 3 grams of the mixture was placed in an α-alumina crucible, which was then placed in an evacuated quartz tube and heated for 1 day at 665 ^{0}C. After cooling to room temperature, the product was ground and identified by X-ray powder diffraction with monochromatized Cu K_α radiation. This procedure was repeated until the X-ray pattern no longer changed. Three heating runs (1+2+2 days) were required to obtain pure $BaAl_{2.5}V_{9.5}F_{9.5}N_{9.5}$, and the corresponding X-ray patterns are shown in Figures 29-32.

X-ray data for the final compound is shown in Table 8 and the corresponding X-ray powder pattern is shown in Figure 32. The data suggests that $BaAl_{2.5}V_{9.5}F_{9.5}N_{9.5}$ exists as a single phase, with a ß-alumina/magnetoplumbite-like structure. The observed c/a ratio of 3.9625 (i.e < 4.0) suggests that the structure is similar to that of magnetoplumbite. In addition, the X-ray data shows the presence of the forbidden reflections (i.e 00ℓ for ℓ = odd) for $P6_3/mmc$. This observation indicates that $BaAl_{2.5}V_{9.5}F_{9.5}N_{9.5}$ behaves similarly to $BaAl_3V_9O_{19}$ in that a superstructure is

TABLE 8

Powder X-Ray Diffraction Data For
$BaAl_{2.5}V_{9.5}F_{9.5}N_{9.5}$.

h	k	ℓ	2θ(cal)	2θ(obs)
*0	0	1	3.75	3.73
0	0	2	7.50	7.49
*0	0	3	11.26	11.26
*0	0	5	18.82	18.79
0	1	2	18.79	18.79
0	1	3	20.61	20.61
0	0	6	22.63	22.68
1	0	4	22.93	22.92
0	1	4	22.93	22.92
0	1	5	25.61	25.51
1	0	5	25.61	25.51
0	1	6	28.58	28.62
0	1	8	35.08	35.06
1	0	8	35.08	35.06
1	1	5	35.68	35.59
0	2	2	36.67	36.65
0	2	6	41.93	41.99
0	2	8	46.84	46.84
0	2	9	49.63	49.64
0	3	2	53.95	53.89
0	3	4	55.75	55.80
0	3	5	57.07	57.17
0	3	7	60.51	60.57
0	3	8	62.60	62.63
0	3	9	64.92	64.94
1	3	5	68.62	68.55
0	4	5	76.69	76.66

* Forbidden reflection for ideal magnetoplumbite structure (space group $P6_3/mmc$).

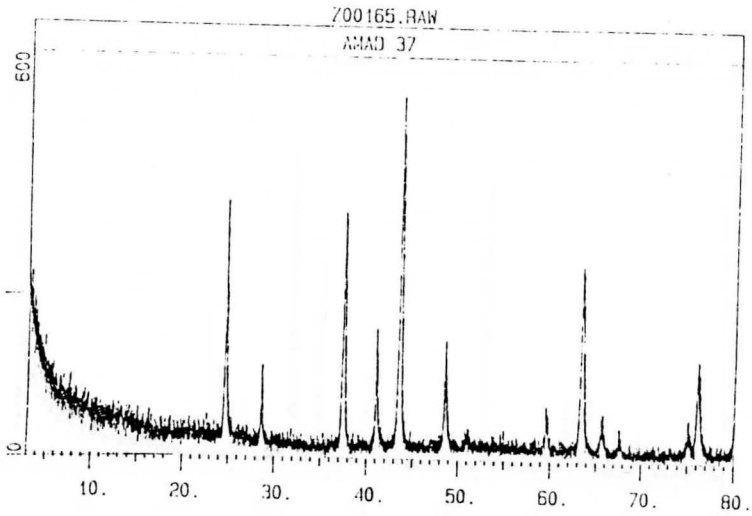

Figure. 29. X-ray pattern for unfired $BaAl_{2.5}V_{9.5}F_{9.5}N_{9.5}$.

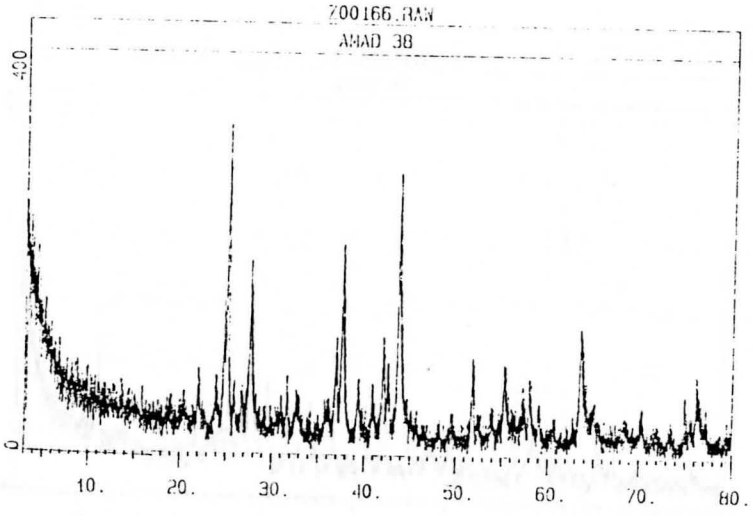

Figure. 30. X-ray pattern of $BaAl_{2.5}V_{9.5}F_{9.5}N_{9.5}$ fired for 1 day.

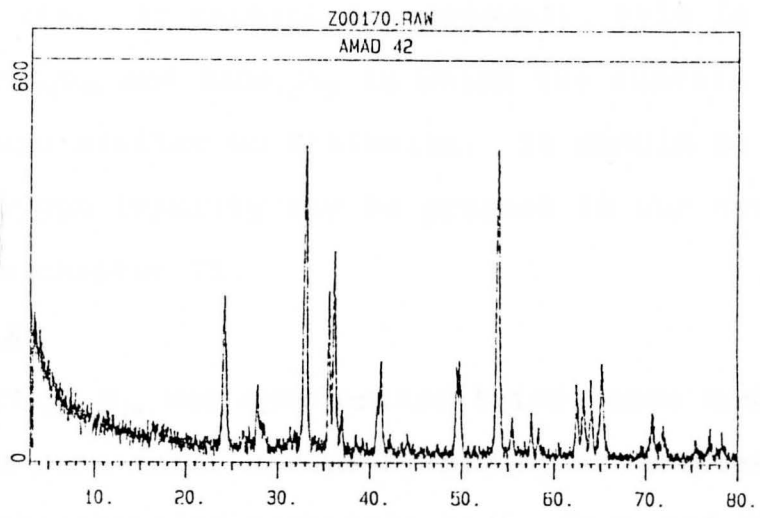

Figure. 31. X-ray pattern for $BaAl_{2.5}V_{9.5}F_{9.5}N_{9.5}$ fired for 3 days.

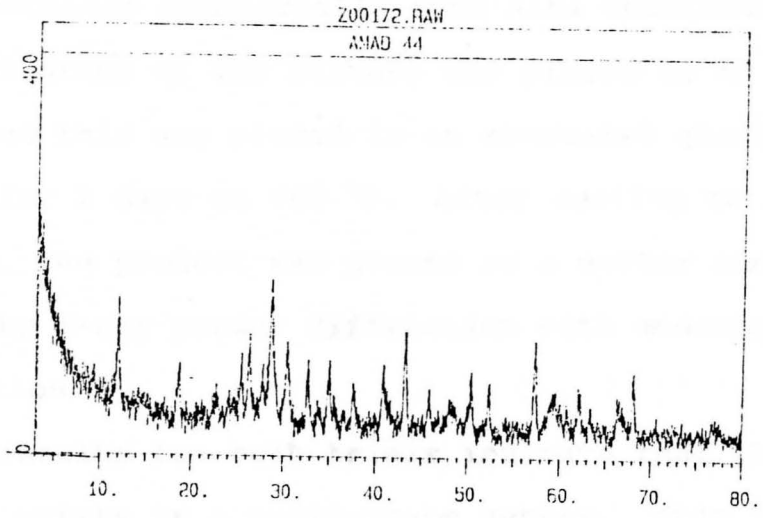

Figure. 32. X-ray pattern for $BaAl_{2.5}V_{9.5}F_{9.5}N_{9.5}$ fired for 5 days.

evident, and the subcell structure is similar to magnetoplumbite. As mentioned previously, this is not the case for $BaAl_{12}O_{19}$ and $BaGa_{12}O_{19}$ in which the subcell structures are similar to ß-alumina. It should be mentioned that some oxygen impurity may be present in our sample, as discussed in chapter VI.

$BaMg_{1.67}Ta_{10.33}N_{19}$

$BaMg_{1.67}Ta_{10.33}N_{19}$ was synthesized twice; once under nitrogen and once under vacuum by mixing stoichiometric amounts of the starting materials Ba_3N_2, Ta_3N_5 and Mg_3N_2 in a 0.333:3.44:0.55 molar ratio. Ta_3N_5 was obtained by reacting $TaCl_5$ under ammonia gas, while slowly increasing the temperature (100 ^{0}C per hr) to 700 ^{0}C. The reaction was kept at 700 ^{0}C for 1 hr to complete the reaction. Ba_3N_2 and Mg_3N_2 were obtained commercially from Alfa Chemicals.

About 3 grams of the mixture was placed in an α-alumina crucible, and this was placed in an evacuated quartz tube and heated for 2 days at 660 ^{0}C. After cooling to room temperature, the product was ground in a mortar and identified by X-ray powder diffraction with monochromatized Cu K_α radiation.

X-ray results for both trials indicate that this composition exists in a multi-phase system. This result was suggested by the presence of a broad peak between the 2θ values of 10 to 20 degrees, as seen in the final X-ray diffraction pattern shown in Figure 34 (cf. 33). The nature of the pattern suggests that the phases could be closely

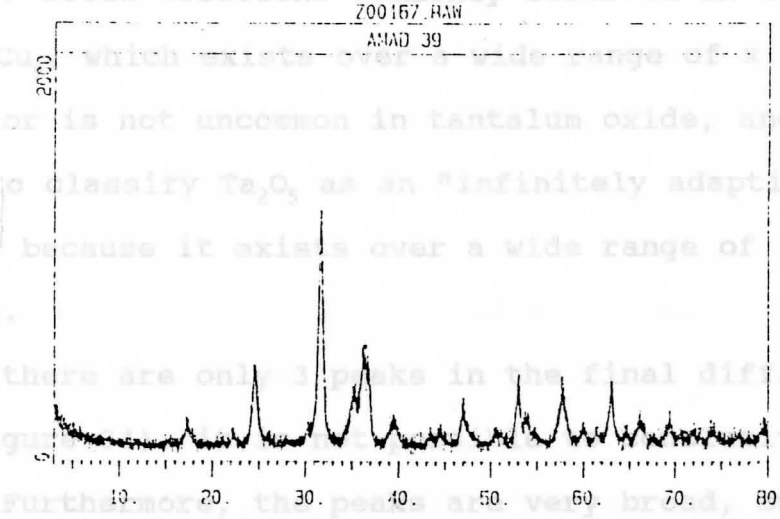

Figure. 33. X-ray pattern of unfired $BaMg_{1.67}Ta_{10.33}N_{19}$.

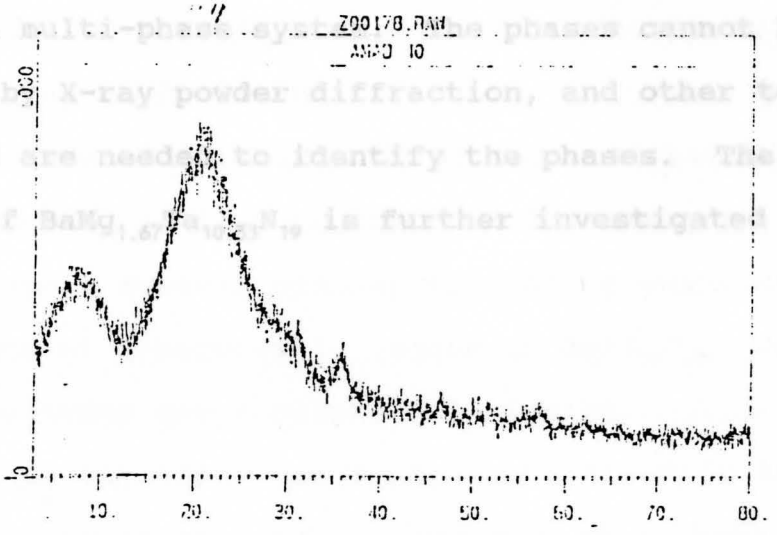

Figure. 34. X-ray pattern for $BaMg_{1.33}Ta_{10.33}N_{19}$ fired for 2 days.

related over a wide range of composition, analogous to the formation of solid solutions commonly observed in alloys such as Au_xCu_y, which exists over a wide range of x and y. Such behavior is not uncommon in tantalum oxide, and led Anderson[23] to classify Ta_2O_5 as an "infinitely adaptive structure", because it exists over a wide range of composition.

Since there are only 3 peaks in the final diffraction pattern (Figure 34), it is not possible to conclusively index it. Furthermore, the peaks are very broad, suggesting a preferred orientation of crystals in the powder sample. Thus, this X-ray powder pattern suggests that $BaMg_{1.67}Ta_{10.33}N_{19}$ cannot exist with the magnetoplumbite structure, but rather exists as a multi-phase system. The phases cannot be identified by X-ray powder diffraction, and other techniques such as TEM are needed to identify the phases. The possible existence of $BaMg_{1.67}Ta_{10.33}N_{19}$ is further investigated in Chapter VI.

Conclusion

From the results presented in Chapter V, it is evident that only certain compounds which ideally have the magnetoplumbite composition and which contain the Ba^{2+} ion in the conduction layers exist with a disordered superlattice similar to that observed in $BaGa_{12}O_{19}$. The only such compounds prepared in this study which have been observed to have the unusual chemistry observed in $BaGa_{12}O_{19}$ are $BaAl_3V_9O_{19}$, $BaFe_3V_9O_{19}$ and $BaAl_{2.5}V_{9.5}F_{9.5}N_{9.5}$. In the case of $BaAl_3V_9O_{19}$ and $BaAl_{2.5}V_{9.5}F_{9.5}N_{9.5}$, it was observed that although both of the above structures behave similarly to $BaGa_{12}O_{19}$ (in that a superstructure is evident), their subcells are apparently similar to magnetoplumbite. This is different than the case for $BaGa_{12}O_{19}$, in which the subcell is more closely related to ß-alumina.

In the case of $BaFe_3V_9O_{19}$, it is evident that a binary phase is present, similar to the case for $BaAl_{12}O_{19}$. One of the phases has a subcell similar to that of magnetoplumbite, with evidence of a supercell. Again in $BaAl_{12}O_{19}$, the subcell structures are similar to ß-alumina.

Regarding the other compounds synthesized in this study, it was found that $BaV_{12}O_{19}$ and $BaFe_3Nb_9O_{19}$ both exist as a binary phase, one of which is similar to ß-alumina. In the case of $BaV_{12}O_{19}$, experimental results reveal that $BaV_{12}O_{19}$ exists with a structure very closely related to that of $BaGa_{12}O_{19}$.

The chart below summarizes the results described for the oxides, and shows data for the prepared compounds.

Compound	Major Phase	c/a	Supercell Present
# $BaAl_{12}O_{19}$	ß-Alumina	4.091	Yes
# $BaGa_{12}O_{19}$	ß-Alumina	4.014	Yes
$BaV_{12}O_{19}$	ß-Alumina	4.194	Yes
$BaAl_3V_9O_{19}$	MP	3.942	Yes
$BaFe_3V_9O_{19}$	MP	3.921	Yes

* MP = Magnetoplumbite.
# Results obtained from Wagner[9].

From the chart, the question as to why $BaV_{12}O_{19}$ should adopt the ß-alumina subcell (like $BaGa_{12}O_{19}$), while $BaFe_3V_9O_{19}$ and $BaAl_3V_9O_{19}$ adopt the magnetoplumbite subcell becomes evident. An explanation for this observation is given by considering the large size of V^{3+} relative to Fe^{3+} and Al^{3+}. Comparison of a and c values for $BaV_{12}O_{19}$ versus $BaGa_{12}O_{19}$ (i.e, for $BaV_{12}O_{19}$ a =5.75 Å, c=24.14 Å and for $BaGa_{12}O_{19}$ a=5.85 Å, c=23.77 Å) shows $BaV_{12}O_{19}$ has an expanded lattice along the c-axis, due to the large size of V^{3+}. If some Al^{3+} replaces V^{3+}, then there will be room on the conduction plane in $BaV_{12}O_{19}$ for positioning of the smaller Al^{3+} ions to reside in. This is possibly the case in $BaAl_3V_9O_{19}$, although a technique such as single crystal X-ray diffraction would be required to verify it.

Meanwhile in the case of $BaFe_3Nb_9O_{19}$, X-ray data reveals the presence of several phases, one of which is a ß-alumina-like phase. This ß-alumina-like phase could have a possible

composition of $BaFe_2Nb^{+2}_5Nb^{+4}_4O_{17}$. None of the other compounds synthesized could have a charge-balanced ß-alumina composition, which partially explains why a supercell forms. In order to determine whether or not the superlattice phase is absent in this compound due to the large size of Nb (relative to Al, Ga, or V), a compound would need to be synthesized for which no charge-balanced ß-alumina composition is possible. This would require Nb_2O_3 as starting material, which is difficult to obtain commercially.

In the case of $BaMg_{1.67}Ta_{10.33}N_{19}$, it was found that a nitride analog to magnetoplumbite with this composition does not exist.

CHAPTER VI

Investigation of the Existence of Nitrides in the Magnetoplumbite/ß-Alumina system Using Bond Valence Analysis.

Introduction

Historically, the bond valence method derives from the Pauling bond number as applied to metals and intermetallic compounds, but was then applied to oxides by Byström and Wilhemm[24] and by Zachariasem[25]. The bond length-bond strength relationship provides a powerful technique for the prediction and interpretation of bond lengths in crystalline solids.

Mathematically, this method can be represented by equations 2 and 3[26]

$$\Sigma_j v_{ij} = v_i \qquad (2)$$

$$v_{ij} = \exp[(R_{ij}-d_{ij})/b] \qquad (3)$$

where v_{ij} is the valence of a bond between two atoms i and j; v_i is the valence of atom i; R_{ij} is the bond valence parameter constant of a bond between two atoms i and j[19] - and it is an empirical parameter, obtained by statistical analysis of all available single structures containing the i-j bond; b is commonly taken to be a universal constant equal to 0.37 Å[26] ; and d_{ij} is the bond length between two

atoms i and j.

According to O'Keeffe[27], there are three well-established uses of the calculation of atomic valences. The first is simply as a check on the accuracy of a structure. The second is to locate atoms such as Mg and Al which are difficult to distinguish by X-ray diffraction, or to distinguish between O, OH and H_2O when H atoms positions are not known. The third use of this method is to distinguish between different oxidation states of transition metal atoms in a given structure. This is performed by a summation of the apparent bond valences for all bonds to a given atom.

For the purpose of this study, equations 2 and 3 were used to calculate predicted bond lengths between pairs of atoms in a structure given ideal bond valences. Once obtained, the bond distances can be compared with previously reported bond distances to predict whether the structure could exist or not. Note that this type of analysis cannot conclusively predict that a certain structure could exist. However, upon finding that a given bond length is much shorter than those typically found for M-X or N-X bonds in $MN_{12}X_{19}$, we could conclude that the structure is not likely to exist.

Predicted Bond Valences and lengths for $BaMg_{1.67}Ta_{10.33}N_{19}$ and $BaAl_{2.5}V_{9.5}F_{9.5}N_{9.5}$.

Using the method described above, values of v_{ij} were obtained for all crystallographically distinct atoms in the ideal magnetoplumbite structure. From the calculated values

of the bond valences, the bond lengths were calculated using the expression proposed by Brown and Altermatt (equation 3)[26].

Note that the composition analyzed, $(BaAl_2V_{10}F_{10}N_9)^+$, differs slightly from the one synthesized, $BaAl_{2.5}V_{9.5}F_{9.5}N_{9.5}$. The reason for this is due to the relative ease of carrying out the calculation for the former composition. For example, it is not possible to distribute fractional atoms (i.e. 9.5 F atoms and 9.5 N atoms) in the 5 crystallographically distinct anionic sites of the magnetoplumbite structure. Of course, in the actual structure, F and N could be distributed in some random fashion throughout all possible anionic sites in some way which preserves the hexagonal symmetry of the system. But the interest in this study lies only in predicting V-F, V-N and Al-F, Al-N bond lengths in an ideal magnetoplumbite structure. The bond valence method can supply this information, even though the composition to be analyzed is not charge balanced.

So, for $[BaAl_2V_{10}F_{10}N_9]^+$, the bond valence sums (of which only 10 are independent) are :

V(1)	$2\alpha+2\beta+\gamma+\delta=3$
Al(1)	$3\epsilon+\zeta=3$
V(2)	$3^n+3\theta=3$
V(3)	$6\iota=3$
V(4)	$2\kappa+3\lambda=3$
Ba	$6\mu+6\nu=2$
N(1)	$2\alpha+\epsilon+\iota=3$
F(1)	$2\beta+^n+\mu=1$
F(2)	$3\gamma+\zeta=1$
N(2)	$3\delta+\kappa=3$
F(3)	$2\theta+\lambda+\nu=1$

Thus for an atom at the V(1) position in the ideal magnetoplumbite structure, there are 6 bonds: 2 of type α, 2 of type ß, 1 of type γ and 1 of type δ. This equation sums to 3, since we expect the valence of V is expected to be +3.

In the magnetoplumbite structure there are 11 different kinds of crystallographically distinct atoms and thus there are 10 independent bond valence sums at the atoms. On the other hand, there are 13 different nearest neighbor bonds. In the above case, two independent equations were required to determine the bond valences, since it was assumed that θ=n and μ=ν, reducing the number of unknowns to 11. This assumption is feasible, since in an ideal structure one expects the bonds from cations to identical anions in a coordination sphere to be as similar as possible. Thus the independent equations are (as obtained from Wagner and O'Keeffe[28]):

$$\epsilon-\zeta+\gamma-\alpha=0$$
$$\mu-\nu+\theta-^{n}=0$$

From these 13 equations, the unknown bond valences were calculated by solving the above equations. The bond lengths were then calculated by using equation 3. Table 9 shows the calculated bond valences and bond lengths for $(BaAl_2V_{10}F_{10}N_9)^+$. These results will be further discussed at the end of this chapter. Again this hypothetical composition is chosen for the purpose of simplifying the calculation.

In the case of $(BaMg_2Ta_{10}N_{19})^-$, the following bond valence sums were needed:

Ta(1)	$2\alpha+2\beta+A+d=5$
Mg	$3\epsilon+X=2$
Ta(2)	$3n+3\theta=5$
Ta(3)	$6\iota=5$
Ta(4)	$2\kappa+3\lambda=5$
Ba	$6\mu+6\nu=2$
N(1)	$2\alpha+\epsilon+\iota=3$
N(2)	$2\beta+n+\mu=3$
N(3)	$3A+X=3$
N(4)	$3d+\kappa=3$
N(5)	$2\theta+\lambda+\nu=3$
	$\epsilon-X+A-\alpha=0$
	$\mu-\nu+\theta-n=0$
	$\nu-d+\kappa-\lambda+\nu-\mu=0$

From these equations, the 13 unknown bond valences were calculated by solving these equations. From these calculated bond valences, the bond lengths were calculated using Equation 3. Table 10 shows the calculated bond valences and bond lengths for $(BaMg_2Ta_{10}N_{19})^-$.

TABLE 9

CALCULATED BOND VALENCES AND BOND LENGTHS IN $(BaAl_2V_{10}F_{10}N_9)^+$.

Bond	Symbol	Valence	* Bond length
V(1)-N(1)	α	0.80303	1.94
V(1)-F(1)	β	0.1666	2.36
V(1)-F(2)	γ	0.2272	2.25
V(1)-N(2)	δ	0.8335	1.92
Al(1)-N(1)	ϵ	0.8939	1.83
Al(1)-F(2)	ζ	0.3181	1.96
V(2)-F(1)	η	1/2	1.95
V(2)-N(3)	θ	1/2	1.95
V(3)-N(1)	ι	1/2	2.11
V(4)-N(2)	κ	0.49938	2.11
V(4)-F(3)	λ	0.66708	2.00
Ba-F	μ	1/6	2.85
Ba-N	ν	1/6	3.13

* Calculated using Eq. 3 and R_{ij} parameters taken from Brese and O'Keeffe[18].

TABLE 10

CALCULATED BOND VALENCES AND BOND LENGTHS IN $(BaMg_2Ta_{10}N_{19})^-$.

Bond	Symbol	Valence	* Bond length
Ta(1)-N(1)	α	0.8333	2.08
Ta(1)-N(2)	ß	0.8935	2.05
Ta(1)-N(3)	A	0.8333	2.08
Ta(1)-N(4)	d	0.7128	2.13
Mg-N(1)	ϵ	0.5	2.11
Mg-N(3)	X	0.5	2.11
Ta(2)-N(2)	n	0.8085	2.09
Ta(2)-N(5)	θ	0.8581	2.07
Ta(3)-N(1)	ι	0.8333	2.08
Ta(4)-N(4)	κ	0.8615	2.07
Ta(4)-N(5)	λ	1.0923	1.98
Ba-N	μ	0.1418	3.19
Ba-N	ν	0.1915	3.08

* Calculated using Eq. 3 and R_{ij} parameters taken from Brese and O'Keeffe[18].

Conclusion

Using the method described earlier in this chapter, the bond valences and bond lengths expected for both $BaAl_{2.5}V_{9.5}F_{9.5}N_{9.5}$ and $BaMgTa_{11}N_{19}$ were calculated. Again, it is important to note that in order to perform the calculations with relative ease, while still obtaining useful results, the hypothetical compositions $(BaAl_2V_{10}F_{10}N_9)^+$ and $(BaMg_2Ta_{10}N_{19})^-$ were used for the bond valance analysis.

Empirical bond valence parameters for nitrides have been reported by Brese and O'Keeffe[19]. The chart on the next page shows the bond valence parameters and bond lengths for certain coordination geometries. Since the bond valence parameter for each coordination geometry (e.g. Al-N in 4-coordination) were obtained by statistical analysis of all relevant single crystal experimental data available in the literature (e.g. , for compounds containing Al-N in 4-coordination), these bond lengths represent the typical "average" bond lengths expected for each type of coordination geometry. Thus comparison of the calculated bond lengths to these "average" bond lengths will provide a good indication as to whether or not the new compounds are likely to exist, as discussed earlier in the chapter.

Bond	R_{ij}	C.N	Bond length
* Al-N	1.79	4	1.89
* Ba-N	2.47	12	3.13
* Mg-N	1.85	4	2.10
* Ta-N	2.01	6	2.07
* Ta-N	2.01	5	2.01
* V-N	1.86	6	2.11
* V-N	1.86	5	2.19
* Al-F	1.54	4	1.65
* Ba-F	2.19	12	2.85
* V-F	1.70	6	1.96
* V-F	1.70	5	1.78

* Reported by Brese and O'Keeffe[19].

$BaAl_{2.5}V_{9.5}F_{9.5}N_{9.5}$ analysis

Using both Table 9 and the above chart, a comparison of lengths calculated for the hypothetical $(BaAl_2V_{10}F_{10}N_9)^+$ compound to the corresponding "average" values above are be performed in the order that they occur in Table 9.

V(1). Four different bond lengths are predicted, of which two are V-N and two are V-F. The calculated average bond length for V(1)-N (1.93 Å) is 0.18 Å shorter than expected (2.11 Å) for V^{+3} coordinated by six Nitrogen atoms. Meanwhile the average calculated V(1)-F (2.30 Å) is 0.34 Å longer than expected (1.96 Å).

Al(1). The average calculated Al(1)-N bond length (1.83 Å) was very close to that expected (1.89 Å). Meanwhile the average calculated Al(1)-F (1.95 Å) is 0.35 Å longer than that expected (1.61 Å).

V(2). Two distinct bond lengths, V(2)-F and V(2)-N

were calculated. The average calculated V(2)-F bond length (1.95 Å) was the same as that reported (1.95 Å). Meanwhile the calculated average of V(2)-N (1.95 Å) was 0.16 Å shorter than that previously reported (2.11 Å).

V(3). The calculated bond length value for V(3)-N (2.11 Å) is the same as the expected value (2.11 Å).

V(4). Since V(4) is on the mirror plane, the coordination figure is a trigonal bipyramid. Theoretically, shorter axial bonds and longer equatorial bonds are expected, however mathematically it is noticed that equatorial bond lengths (2.0 Å) are shorter than the axial bond length (2.11 Å).

Ba. The barium coordination is that of a twinned cuboctahedron. The calculated Ba-F bond length (2.85 Å) agrees with the expected length (2.85 Å). Also the calculated Ba-F bond length (3.13 Å) agrees with the expected average length (3.13 Å).

Hypothetically by using the comparison described above, it can be predicted that $BaAl_{2.5}V_{9.5}F_{9.5}N_{9.5}$ might exist as a magnetoplumbite, in spite of the shorter-than-predicted bond lengths at the V(1) and V(2) positions. The reason for this is that V^{+3} has a d^2 configuration, and is therefore subject to small Jahn-Teller distortions. Thus, the phase may exist, but with slight distortions at the V coordination spheres. However, one cannot rule out the possibility that $BaAl_{2.5}V_{9.5}F_{9.5}N_{9.5}$ does not exist as an ideal magnetoplumbite structure, and that our successfully prepared compound is

actually stabilized with oxygen. Since the sample was prepared in a vacuum, the source of oxygen impurity could be the alumina boat containing the sample. Whether or not this is the case will be determined by microanalysis at a future date, when the resources become available. Also, similar reactions in the future will be conducted using a platinum crucible, which was not available at the time this work was done.

$BaMg_{1.67}Ta_{10.33}N_{19}$ analysis

The analysis was carried on the hypothetical composition $[BaMg_2Ta_{10}N_{19}]^-$, the length of the bonds to the metal atom is discussed in the order they occur in Table 10.

Ta(1). We predict four different bond lengths with a range of 0.08 Å. The average calculated bond length for Ta(1)-N (2.08 Å) is 0.01 Å longer than that expected (2.07 Å).

Mg. The calculated bond length for Mg-N (2.11 Å) is very close to the average value calculated by O'Keeffe (2.10 Å)[18].

Ta(2). The two distinct Ta-N are calculated to have the bond valences expected for regular octahedral coordination (0.833). Therefore the calculated average bond length (2.075 Å) is the same as predicted by O'Keeffe (2.07 Å)[18].

Ta(3). There is by symmetry only one independent Ta(3)-N bond length. The calculated and predicted values

are the same (2.08 Å).

Ta(4). Since Ta(4) is on the mirror plane, the coordination polyhedron is a trigonal bipyramid. Therefore, it is expect that shorter equatorial (1.98 Å) and longer axial (2.09 Å) bond lengths than the Ta-N bond length predicted by O'Keeffe (2.08 Å)[18].

Ba. The barium coordination is that of twinned cuboctahedron. The average calculated bond length for Ba-N (3.13 Å) is the same as the average length reported by O'Keeffe[18].

From the results described above, by comparing both the average calculated bond length from this work to those bond lengths reported by O'Keeffe[19], it can be predicted that $BaMg_{1.67}Ta_{10.33}N_{19}$ might exist as a magnetoplumbite. However, one must keep in mind that the bond valence analysis method is most valuable in predicting which compounds cannot exist. The conclusion here indicates that $BaMg_{1.67}Ta_{10.33}N_{19}$ with a magnetoplumbite structure would have bond lengths compatible with similar types of bonds observed in other compounds. This method does not take into account the role of thermodynamics in determining the existence of a certain phase. Thus one is left with two possible conclusions: 1) $BaMg_{1.67}Ta_{10.33}N_{19}$ does not exist (i.e. for thermodynamic reasons) or 2) The attempt to synthesize the phase was unsuccessful, but future attempts to synthesize it could be successful.

Future Work

The most obvious future work which could be done on the compounds synthesized in this work is analysis utilizing transmission electron microscopy (TEM). TEM analysis would reveal the phase relationships in those compounds which have more than one phase, and would also elucidate the nature of the defects responsible for presence of forbidden reflections observed in the X-ray data of these compounds. This work is planned in the future, when the TEM available in the Chemistry Department becomes operable.

Future work should also include elemental analysis of the compounds synthesized in this study, particularly in the case of the nitride-fluoride compound prepared. It is important to determine whether or not any oxygen is present in the lattice of this compound, and also to determine whether N_2 was lost during the synthesis.

It would be interesting in future work to prepare a composition containing Nb^{3+}, such as $BaNb_{12}O_{19}$. If this compound exists in the ß-alumina/magnetoplumbite system, one would probably not expect to observe superlattice formation due to the large size of Nb relative to Al, Ga, or V.

Other work could focus on preparing single crystals of composition $MR_{11}X_{17}$ or $MR_{12}X_{19}$, where M = Na, K, Sr, Ca, or Ba; R = Al and/or combinations of Mg, Sc, Fe, V, Nb, Ta, Fe, Ga or Si; and X = O or N or F or a combination of F and N. Once synthesized they could be characterized by single crystal X-ray analysis, and the results could be used to

determine the extent to which the unusual chemistry observed in $BaGa_{12}O_{19}$ depends upon composition, size and identity of the large cation present.

Other related work could focus on the study of the physical properties of the newly synthesized compounds. These properties includes optical composition, laser emission cross section, fracture strength, thermal conductivity and stability.

REFERENCES

1. A. R. West "Basic Solid State Chemistry", 2nd ed., John Wiley and Sons Ltd, New York (1988).

2. W. F. Smith "Principles of Materials Science and Engineering", 3rd ed. McGraw-Hill Book Company, New York (1986).

3. G. A. Rankin and H. E. Merwin, J. Amer. Chem. Soc. **38**, 568 (1916).

4. C. W. Stillwell, J. Phys Chem. **30**, 1441 (1926).

5. W. L. Bragg, C. Gottfried and J. West, Z. Krist. **77**, 255 (1931).

6. C. A. Beevers and M. A. Ross, Z. Krist. **97**, 59 (1937).

7. J. T. Kummer and N. Weber, Soc. Automot. Eng. Trans. **76**, 1003 (1967).

8. J. D. Bates, J. C. Wang and N. J Dudney, Physics Today. July, 46 (1982).

9. T. R. Wagner, Ph.D. Thesis, Arizona State University, (1986).

10. C. R Peters, M. Bettman, J. W. Moore and M. D. Glick, Acta Cryst. **B27**, 1826 (1971).

11. S. B. Hendricks and L. Pauling, Z. Krist. **64**, 303 (1927).

12. G. Aminoff, Geol. Fören. Förh. **47**, 283 (1925).

13. V. Adelsköld, Arkiv. Kemi. Mineral Geol. **12**, 9 (1938).

14. N. Iyi, Z. Inoue, S. Takekawa and S. Kimura, J. Solid State Chem. **60**, 61 (1985).

15. T. R. Wagner and M. O'Keeffe, J. Solid State Chem. **73**, 19 (1988).

16. Y. Kanke, F. Izumi, Y. Morii, S. Funahashi and K. Kato, J. Solid State Chem. **104**, 319 (1993).

17. F. J. Disalvo, Science. **247**, 649 (1990).

18. N. E. Brese and M. O'Keeffe, Structure and Bonding. **79**, 303 (1992).

19. N. E. Brese and M. O'Keeffe, Acta Cryst. **B47**, 1992 (1991).

20. J. T. Kummer "Progrees in Solid State Chemistry", Vol. 7, Reiss and McCaldin Eds. , New York (1972).

21. J. M. Newsam and B. C. Tofield, Solid State Ionics. **5**, 59 (1981).

22. J. B. Boilot, G. Colliin, P. H. Colomban and R. Comes, Solid State Ionics. **5**, 157 (1981).

23. J. S. Anderson, J. Chem. Soc. Datton Trans. 1107 (1973).

24. A. Byström and K. A. Wilhelmli, Acta. Chem. Scand. **5**, 1003 (1951).

25. W. H. Zachariasen, Acta Cryst. **16**, 385 (1963).

26. I. D. Broun and D. Altermatt, Acta Cryst. **B41**, 244 (1985).

27. M. O'Keeffe, Structure and Bonding. **71**, 161 (1989).

28. T. R. Wagner and M. O'Keeffe, J. Solid State Chemistry. **73**, 211 (1988).